Structural modeling reveals the mechanism of motor ATPase coordination during type IV pilus retraction

Abigail E. Teipen[1], Jacob D. Holt[2,3], Diane L. Lynch[4,5], Yixuan Peng[2,3], Triana N. Dalia[1], James C. Gumbart[4,5,*], Carey D. Nadell[2,3,*], Ankur B. Dalia[1,*]

[1]Department of Biology, Indiana University, Bloomington, IN 47405
[2]Department of Biological Sciences, Dartmouth, Hanover, NH 03755
[3]Department of Microbiology and Immunology, Geisel School of Medicine at Dartmouth, Hanover, NH 03755
[4]School of Physics, Georgia Institute of Technology, Atlanta, Georgia 30332
[5]School of Chemistry & Biochemistry, Georgia Institute of Technology, Atlanta, Georgia 30332

*To whom correspondence may be addressed. Email: ankdalia@iu.edu, carey.d.nadell@dartmouth.edu, and gumbart@physics.gatech.edu

ABSTRACT

Diverse bacterial species utilize surface appendages called type IV pili (T4P) to interact with their environment. These structures are dynamically extended and retracted from the cell surface, which is critical for diverse functions. Some T4P systems rely on two distinct motor ATPases, PilT and PilU, whose combined activities are required to power forceful T4P retraction. However, the mechanism by which these motors coordinate to facilitate T4P retraction has remained unclear. Here, we utilize the competence T4P in *V. cholerae* as a model system to elucidate the molecular basis for PilT-PilU coordination during T4P retraction. Specifically, we modeled the interactions between PilT and PilU using AlphaFold 3 and molecular dynamics (MD) simulations. We then empirically tested these models using a combination of cytological and high-resolution genetic approaches. Our results reveal that interactions between PilT and the PilU C-terminus are critical for these motors to coordinate to drive T4P retraction. Finally, we show that PilT-PilU interactions are broadly conserved in T4P systems from diverse bacterial species, and we experimentally validate that they are required for T4P retraction in *Acinetobacter baylyi*. Together, this work expands our fundamental understanding of T4P dynamics, and more broadly it provides mechanistic insight into how these ATPases coordinate to assemble some of the strongest biological motors in nature.

SIGNIFICANCE

Diverse bacterial species use filamentous surface appendages called type IV pili (T4P) to move along surfaces, take up DNA for horizontal gene transfer, and stick to biotic and abiotic surfaces. The forceful retraction of these filaments is often required for these behaviors. In many T4P systems, the combined activity of two distinct motor ATPase proteins is required for forceful retraction; however, a detailed understanding of *how* these motor proteins interact to promote forceful retraction is currently lacking. Here, we use an integrated approach to uncover the molecular mechanism for motor ATPase coordination. Furthermore, we show that this mechanism is broadly conserved in diverse T4P systems.

INTRODUCTION

Type IV pili (T4P) are broadly conserved proteinaceous surface appendages that mediate several important behaviors including DNA uptake for natural transformation, surface attachment, surface sensing, and twitching motility (1-5). The T4P machine is a large macromolecular complex composed of at least 80 proteins (via a multimeric assembly of 7 unique proteins) (6-8). This nanomachine dynamically assembles (extends) and disassembles (retracts) a pilus fiber through an outer membrane gated secretin (9, 10), and this dynamic extension and retraction is critical for the diverse functions carried out by T4P (2, 4, 11).

In canonical T4P (*i.e.*, type IVa pilus systems), dynamic extension and retraction are powered by distinct hexameric motor ATPases. Pilus extension is often driven by a single motor ATPase protein, PilB, that interacts with the T4P platform protein, PilC, and hydrolyzes ATP to power the assembly of major pilin subunits into a helical pilus filament that extends from the cell surface through the outer membrane secretin, PilQ (12, 13). Conversely, T4P retraction is commonly powered by two distinct motor ATPases – PilT and PilU. Previous studies have established that PilT serves as the primary retraction ATPase (12, 14, 15) that directly interacts with PilC to promote depolymerization of major pilin subunits. PilU is an accessory ATPase (16, 17) that drives forceful T4P retraction in a PilT-dependent manner (18-20). A detailed mechanistic understanding of *why* PilU requires PilT to promote retraction and *how* PilT and PilU coordinate to promote forceful T4P retraction, however, remains unclear.

In this study, we use the *Vibrio cholerae* competence T4P as a model system to dissect the molecular mechanism underlying PilT-PilU-mediated retraction. The *V. cholerae* competence T4P is required for DNA uptake during horizontal gene transfer by natural transformation (NT) (1). During this process, competence T4P extend from the bacterial surface, bind to DNA in the environment, and then retract to bring this DNA into the cell (11, 21). This DNA is then translocated into the cytoplasm and if it is homologous to the host genome, it can be integrated by homologous recombination (22). NT is induced when *V. cholerae* colonizes the chitinous shells of crustacean zooplankton in the aquatic environment (23). Recent work highlights that PilU-dependent retraction is necessary for NT when DNA is adsorbed to a chitin surface (24). Thus, PilT and PilU are both critical for facilitating DNA uptake by competence T4P under physiologically relevant conditions. Also, the *V. cholerae* competence T4P has emerged as an invaluable model system for studying the basic biology of T4P (11, 18, 19, 25-27). Thus, it is ideally suited for dissecting the molecular mechanism underlying PilT-PilU coordination during T4P retraction.

RESULTS

AlphaFold 3 models interactions between the retraction motor ATPases and the T4P machine

To define how PilT and PilU coordinate to facilitate T4P retraction, we first sought to model their interactions with PilC using AlphaFold 3 (AF3) (28). Due to the large size of this complex, we

generated a hybrid model of PilC-PilT-PilU by independently modeling the interaction between 1) PilC and the PilT hexamer and 2) the PilT and PilU hexamers (**Fig. S1a-b**). Then, one subunit of PilT was aligned between these two models to generate the hybrid complex (**Fig. 1a**).

The relatively high model confidence scores for PilT-PilC (ipTM = 0.66) and PilT-PilU (ipTM = 0.63) suggest that PilT may directly interact with both PilC and PilU (**Fig. S1a-b**). By contrast, AF3 modeling of PilU-PilC yields very low confidence models (ipTM = 0.37), which suggests that PilU and PilC may not directly interact (**Fig. S1c**). Because PilT is predicted to interact with PilC and PilU via distinct interfaces (**Fig. 1a**), we hypothesize that PilU requires PilT to engage the T4P machine. This model is consistent with prior work demonstrating that PilU can only facilitate T4P retraction in the presence of PilT (18, 19, 26).

PilT bridges PilU to the T4P machine

To test whether PilU requires PilT to engage the membrane-embedded T4P machine, we sought to develop an assay to examine the interaction of these ATPases with the T4P machine in live cells. When the ATPase activity of these motors is intact (*pilT*$^{+}$ and/or *pilU*$^{+}$), it is likely that they only engage the T4P machine transiently while actively promoting T4P retraction. Accordingly, strains expressing *mCherry-pilT*$^{+}$ and *mCherry-pilU*$^{+}$ do not form foci at the cell periphery (**Fig. S2, Movies S1 and S2**). We hypothesized that we could stabilize the interaction of these ATPases with the T4P machine by ablating their ATPase activity via mutation of the Walker A (WA) site required for ATP-binding (*pilT*^{WA} = *pilT*^{K136A}; *pilU*^{WA} = *pilU*^{K134A}) (18, 29) (**Fig. S1b**). Indeed, in strains expressing *mCherry-pilT*^{WA} *pilU*^{WA} and *pilT*^{WA} *mCherry-pilU*^{WA}, fluorescent foci are readily observed at the cell periphery in the majority of cells (**Fig. 1b-d, Fig. S2c, Movies S3 and S4**). Also, these peripheral foci exhibited low mobility (**Fig. S2b**), which is consistent with these peripheral foci representing T4P machine-engaged motor ATPases. PilT and PilU can promote retraction of both the competence T4P and the MSHA T4P in *V. cholerae* (19, 30, 31) via interactions with the platform protein of each system (*pilC* and *mshG*, respectively). In a background where these platform proteins are deleted, mCherry-PilT^{WA} and mCherry-PilU^{WA} foci are ablated (**Fig. 1c-d**). This supports the hypothesis that the peripheral *mCherry-pilT*^{WA} and *mCherry-pilU*^{WA} foci observed in the parent represent T4P machine-engaged motors. To further test this hypothesis, we assessed whether these motor foci colocalize with the T4P machine. Specifically, we assessed the colocalization of mCherry-PilT^{WA} and mCherry-PilU^{WA} with competence T4P filaments and a competence T4P machine component (*msfGFP-pilQ*) in a background where the MSHA locus has been deleted (*ΔMSHA*), which ensures that motors can only interact with competence T4P machines. Qualitatively, we found that mCherry-PilT^{WA} and mCherry-PilU^{WA} foci colocalized with the base of extended competence T4P (**Fig. S3a, Movies S5 and S6**). Also, more quantitatively, we determined that mCherry-PilT^{WA} and mCherry-PilU^{WA} foci colocalize with msfGFP-PilQ foci at a frequency of 99.3 ± 0.7% and 98.1% ± 1%, respectively (**Fig. S3b-c, Movies S7 and S8**). All together, these results strongly suggest that mCherry-PilT^{WA} and mCherry-PilU^{WA} foci represent motor ATPases that are bound to a T4P machine.

The AF3 model suggests that PilT directly interacts with the T4P machine; thus, we hypothesized that PilU would be dispensable for PilT-T4P interactions. Consistent with this, *mCherry-pilT*^{WA} Δ*pilU* cells still readily formed fluorescent foci (**Fig. 1c**). Importantly, deletion of the T4P

platform proteins still ablates focus formation in this background (**Fig. 1c**). By contrast, the AF3 model suggests that PilT is required to bridge the interaction between PilU and the T4P machine (**Fig. 1a**). Indeed, fluorescent foci are ablated in *mCherry-pilU*^{WA} Δ*pilT* compared to the *mCherry-pilU*^{WA} *pilT*^{WA} parent (**Fig. 1d**). Together these results indicate that PilT may directly interact with the T4P machine, and that PilT is required to bridge PilU-T4P interactions.

The AF3 model also predicts a direct interaction between PilT and PilU. Accordingly, in *pilT*^{WA}-*mCherry gfp-pilU*^{WA} cells, 96% ± 2% of the GFP-PilU^{WA} foci overlap with a PilT^{WA}-mCherry focus (**Fig. 1e, Movie S9**). Additionally, both PilT^{WA}-mCherry and GFP-PilU^{WA} foci primarily localize to the cell poles (**Fig. 1f**) where T4P machines are most prevalent (**Fig. S3b-c**). This colocalization is consistent with these ATPase motors interacting at the same T4P machine as suggested by the AF3 model.

Our data thus far strongly suggest that PilT and PilU interact with one another to engage the T4P machine, which is consistent with the AF3 model. This is also supported by a recent preprint that analyzes the *V. cholerae* competence T4P machine *in situ* via cryo-EM. In strains expressing *pilT*^{WA} and *pilU*^{WA}, subtomogram averages revealed the presence of two stacked densities below the T4P machine that nicely fit the PilT-PilU AF3 model (32), which is consistent with stacked PilT and PilU hexamers engaging the T4P machine. Altogether, these results support the ultrastructural organization of the PilC-PilT-PilU complex predicted by the AF3 hybrid model.

Interactions between PilT and the PilU$^{C\text{-}term}$ are critical for T4P retraction

Our data thus far suggest that PilT and PilU interact and that this interaction is likely required for PilU to engage the T4P machine. Next, we sought to employ the PilT-PilU AF3 model to further define the molecular basis for motor ATPase coordination.

Competence T4P retraction is necessary for DNA uptake (1, 11); thus, NT serves as a simple, yet sensitive readout (>5-logs of dynamic range) for T4P retraction (**Fig. 2b**). Competence T4P can also be directly imaged in *V. cholerae* via introduction of a cysteine into the major pilin (*pilA*^{S67C}), which allows for subsequent labeling with fluorescent maleimide dyes (11, 33). Strains that are competent for T4P retraction have very few extended pili because competence T4P are highly dynamic (**Fig. 2c**, parent). In contrast, strains that cannot retract competence T4P become hyperpiliated due to the accumulation of static extended pili on the cell surface (**Fig. 2c**, Δ*pilT*). Competence T4P also self-interact (27); thus, hyperpiliated cells form large multi-cellular aggregates that "floc" out of solution (**Fig. 2c**) (18). PilU is normally dispensable for competence T4P retraction, however, if cells contain a PilT^{WA} mutation, retraction becomes dependent on PilU (18, 19), a finding that we recapitulate here (**Fig. 2b-c**, compare Δ*pilU* to *pilT*^{WA} Δ*pilU*). Thus, the *pilT*^{WA} background can be used to assess PilT-PilU-dependent retraction (*i.e.*, retraction that is dependent on <u>both</u> motor ATPases), while a background where PilT ATPase activity is intact and *pilU* is deleted (*pilT*$^{+}$ Δ*pilU*) can be used to assess PilT-dependent retraction (*i.e.*, retraction that is only dependent on PilT). For this reason, we initially focused on mutating the PilT side of the PilT-PilU interface to define regions that are 1) critical for these motors to coordinate and promote PilT-PilU-dependent T4P retraction but 2) dispensable for PilT-dependent retraction.

Analysis of the AF3 model revealed three distinct regions of PilT that putatively form salt bridges with PilU – PilT^{D2,E53}, PilT^{R35,K36}, and PilT^{E64,E65} (**Fig. 2a and Fig. S4**). To test if any of these areas are required for PilT-PilU-dependent retraction, we mutated these PilT residues to alanines and assessed pilus retraction using NT, direct observation of competence T4P, and cellular aggregation as described above. The phenotype of *pilT^{WA,E64A,E65A}* was indistinguishable from *pilT^{WA}*, suggesting that this region is dispensable for PilT-PilU-dependent retraction (**Fig. 2b-c**). By contrast, *pilT^{WA,R35A,K36A}* and *pilT^{WA,D2A,E53A}* resulted in an ~3.5-log decrease in NT (compared to *pilT^{WA}*) and a strong hyperpiliation and aggregation phenotype which is consistent with these two regions playing an important role in PilT-PilU-dependent retraction (**Fig. 2b-c**). Importantly, mutating these three regions (*pilT^{E64A,E65A}*, *pilT^{D2A,E53A}*, and *pilT^{R35A,K36A}*) does not diminish PilT-dependent T4P retraction (*i.e.*, retraction in a *pilT*$^{+}$ Δ*pilU* background), indicating that PilT^{D2,E53} and PilT^{R35,K36} are specifically required for PilT-PilU-dependent retraction (**Fig. 2b-c**).

The reduction in PilT-PilU-dependent retraction observed in *pilT^{D2A,E53A}* and *pilT^{R35A,K36A}* may be due to an effect of these mutations on either (1) diminishing PilT-PilU interactions or (2) preventing PilT-PilU coordination without affecting their interaction. To distinguish between these, we assessed the effect of these mutations on PilT and PilU localization to T4P machines. We hypothesized that if these regions are required for PilT-PilU interactions, mutating these residues in a *pilT^{WA} mCherry-pilU^{WA}* background would result in loss of mCherry-PilU^{WA} foci. When we performed this analysis, *pilT^{WA,D2A,E53A} mCherry-pilU^{WA}* and *pilT^{WA,R35A,K36A} mCherry-pilU^{WA}* no longer formed mCherry-PilU^{WA} foci (**Fig. 2d**). While *pilT^{WA,D2A,E53}* and *pilT^{WA,R35A,K36A}* do not completely eliminate PilT-PilU-dependent transformation (**Fig. 2b-c**); transformation is still reduced ~1000-fold. Thus, while there is likely still some residual PilT-PilU interactions in these backgrounds, it is below the limit of detection of our microscopy-based motor localization assay which inherently has a narrower dynamic range. By contrast, *pilT^{WA,E64A,E65A} mCherry-pilU^{WA}* still formed mCherry-PilU^{WA} foci and was indistinguishable from the *pilT^{WA} mCherry-pilU^{WA}* parent (**Fig. 2d**), which is consistent with this mutation having no effect on PilT-PilU-dependent retraction (**Fig. 2b-c**). Importantly, mCherry-PilT^{WA,E64A,E65A}, mCherry-PilT^{WA,D2A,E53A}, and mCherry-PilT^{WA,R35A,K36A} all localized to T4P machines just like the mCherry-PilT^{WA} parent (**Fig. 2e**), which is consistent with these mutations having no effect on PilT-dependent retraction (**Fig. 2b-c**). Together, these data suggest that PilT^{D2,E53} and PilT^{R35,K36} are important for the interaction between PilT and PilU that allow this complex to coordinate retraction.

PilT^{D2,E53} and PilT^{R35,K36} are both predicted to interact with the PilU C-terminus (PilU$^{C\text{-}term}$). PilT and PilU are highly homologous motor ATPases, however the extended C-terminal domain is a unique feature of PilU homologs (**Fig. S5**)**.** The AF3 model predicts that the PilU$^{C\text{-}term}$ wraps around the sides of the PilT hexamer (**Fig. 2a**). Because our mutational analysis demonstrates that PilT^{D2,E53} and PilT^{R35,K36} diminish PilT-PilU-dependent retraction (**Fig. 2**), we hypothesized that interactions between PilT and the PilU$^{C\text{-}term}$ are critical for PilT-PilU mediated T4P retraction.

To test this hypothesis at a higher resolution, we targeted the putative intermolecular salt bridges formed between PilT^{D2,E53}-PilU^{K348}, PilT$^{R35\text{-}}$PilU^{D366,E368}, PilT^{K36}-PilU^{D366} for mutagenesis by flipping their charge (**Fig. 3a**). We reasoned that flipping the charge on either side of the

intermolecular salt bridge should have a repulsive effect that breaks PilT-PilU interactions, which should disrupt pilus retraction. However, flipping the charge on both sides of the salt bridge should repair the interaction and restore T4P retraction. Importantly, restoration of T4P retraction in the double charge-flip mutant should only occur if the two residues interact, thus, providing an easy genetic approach for testing the residue-level accuracy of the PilT-PilU interactions predicted by AF3.

As shown above, mutating the PilT side of the interface allows us to test whether mutations specifically affect PilT-PilU-dependent retraction (tested in the *pilT*^{WA} background) without disrupting PilT-dependent retraction (tested in the *pilT*$^{+}$ Δ*pilU* background). By contrast, mutating the PilU side of the interface cannot distinguish between 1) disruption of the PilT-PilU interface and 2) mutations that decrease PilU stability or cause it to misfold. Thus, we first assessed the impact of flipping the charge on the PilT side of the interface in the three predicted salt bridge contacts (*pilT*^{R35E}, *pilT*^{K36E}, and *pilT*^{D2K,E53R}). All three mutants resulted in a decrease in NT, with *pilT*^{R35E} and *pilT*^{D2K,E53R} causing the most severe loss of retraction (**Fig. 3b-c**). Importantly, these mutations had no observable impact on PilT-dependent retraction (**Fig. S6**). Thus, disrupting the PilT side of the putative PilT^{D2,E53}-PilU^{K348}, PilT^{R35}-PilU^{D366,E368}, and PilT^{K36}-PilU^{D366} salt bridges specifically inhibited PilT-PilU-dependent T4P retraction.

To further probe the validity of these intermolecular salt bridges, we sought to flip the charge on the PilU side of the interface to test whether this recovered T4P retraction. The AF3 model indicates that PilT^{R35} makes contacts with both PilU^{D366} and PilU^{E368} (**Fig. 3a**). The *pilT*^{WA,R35E} *pilU*^{D366K,E368K} strain, however, remained hyperpiliated and only had a modest ~1 log restoration in NT when compared to *pilT*^{WA,R35E} *pilU*^{WT} (**Fig. 3b-c**). Importantly, *pilU*^{D366K,E368K} did not affect steady-state levels of PilU (**Fig S7a**). Together, these results suggest that PilT^{R35} does not form a salt bridge with PilU^{D366,E368}. To more rigorously examine the stability of these putative intermolecular salt bridges, we performed all-atom molecular dynamics (MD) simulations of the PilT-PilU AF3 model. The resulting 500-ns MD simulations were then analyzed to determine the percent of time that residues remained in close enough proximity to form a salt bridge (<3.5 Å), with a higher percentage indicating a more stable interaction. The AF3-MD simulations indicated that PilT^{R35} was not predicted to form a stable interaction with either PilU^{D366} or PilU^{E368} (**Fig. 3d**, **S8**, and **Movie S10**). Thus, while PilT^{R35} is clearly critical for PilT-PilU-dependent retraction, it likely does not form a salt bridge with PilU. Instead, PilT^{R35} may promote PilT-PilU interactions via other intermolecular contacts. Accordingly, the MD simulation suggests that PilT^{R35} interacts with PilU^{I365} and PilU^{M367} (**Fig. S9** and **Movie S11**).

For PilT^{K36}, the AF3-MD simulation predicted a stable salt bridge for PilT^{K36}-PilU^{D366} (**Fig. 3d**, **S8**, and **Movie S12**). Consistent with this, introducing *pilU*^{D366K} into the *pilT*^{WA,K36E} background restored T4P retraction to parent levels (**Fig. 3b-c**). Importantly, steady-state levels of PilU^{D366K} are similar to the PilU^{WT} parent (**Fig S7a**). If PilT^{K36} and PilU^{D366} exclusively form a salt bridge, a charge flip mutation to either residue should result in a similar transformation deficit. Unlike *pilT*^{WA,K36E}, however, *pilT*^{WA} *pilU*^{D366K} transforms like the parent (**Fig. 3b-c**). This suggests that PilT^{K36} may form additional contacts with PilU. The AF3-MD simulations suggest that PilT^{K36} may interact with PilU^{E368}; and these interactions were not altered when we performed MD

simulations of the PilT-PilU^{D366K} complex (**Fig. S10**). Based on this, we hypothesized that PilT^{K36}-PilU^{E368} may partially compensate for the loss of PilT^{K36}-PilU^{D366} interactions in the PilU^{D366K} background. Consistent with this, *pilT^{WA} pilU^{D366K,E368K}* exhibited a ~2-log transformation deficit compared to *pilT^{WA} pilU^{D366K}* (**Fig. 3b**). If this difference is due to the loss of residual PilT^{K36}-PilU^{E368} interactions, then we hypothesized that the transformation deficit of *pilT^{WA} pilU^{D366K,E368K}* should be completely restored to parent levels in *pilT^{WA,K36E} pilU^{D366K,E368K}* (similar to what is observed for *pilT^{WA,K36E} pilU^{D366K}*). Indeed, *pilT^{WA,K36E} pilU^{D366K,E368K}* exhibited a transformation phenotype that was indistinguishable from the parent (**Fig. 3b**). Thus, PilT^{K36} likely interacts with both PilU^{D366} and PilU^{E368}; with PilT^{K36}-PilU^{D366} interactions playing the dominant role since recovery of transformation is greater in *pilT^{WA,K36E} pilU^{D366K}* than in *pilT^{WA,K36E} pilU^{E368K}* (**Fig. 3b**).

For PilT^{D2,E53}, the AF3-MD simulation predicted a stable salt bridge between PilT^{D2,E53}-PilU^{K348}, with all three residues participating in the interaction (**Fig. 3d**, **S8**, and **Movie S13**). Accordingly, *pilT^{WA,D2K,E35R} pilU^{K348D}* largely restored NT and surface piliation when compared to *pilT^{WA,D2K,E35R} pilU^{WT} and pilT^{WA} pilU^{K348D}* (**Fig. 3b-c**). Importantly, steady-state levels of PilU^{K348D} are similar to the PilU^{WT} parent (**Fig. S7a**).

Together, these results help further validate the AF3 model and demonstrate that PilT-PilU$^{C\text{-}term}$ interactions are critical for PilT-PilU-dependent retraction at the molecular scale.

PilT-PilU$^{C\text{-}term}$ contacts are necessary for the high retraction forces needed for NT under physiologically relevant conditions

Thus far, we have used the *pilT^{WA}* background to isolate and study PilT-PilU-dependent retraction, but when PilT ATPase activity is intact, PilU is dispensable for competence T4P retraction. Accordingly, Δ*pilU* can take up soluble transforming DNA (tDNA) from the environment at a similar frequency to the parent (**Fig. 2b** and **4a**). PilU, however, is critical for generating high retraction forces (18, 20). We recently demonstrated that PilU-dependent retraction is necessary for NT when tDNA is adsorbed to a chitin surface (24), a finding that we recapitulate here (**Fig. 4b-c**). Thus, assessing NT of *V. cholerae* in chitin biofilms under flow allows us to study PilT-PilU-dependent retraction in a physiologically relevant setting.

Based on the results described above, we hypothesized that PilT-PilU$^{C\text{-}term}$ contacts would be critical for coordinating the forceful T4P retraction required for NT in chitin flow biofilms when tDNA is adsorbed to chitin. Consistent with this, *pilT^{R35E}*, the single charge-flip mutation that had the strongest impact on PilT-PilU-dependent retraction (**Fig. 3b**), exhibited a loss in NT that was indistinguishable from Δ*pilU* when tDNA was adsorbed to chitin (**Fig. 4b-c**). Importantly, the ATPase activity of both PilT and PilU are intact in this mutant; thus, the disruption of PilT-PilU$^{C\text{-}term}$ interactions in *pilT^{R35E}* likely disrupts the ability of PilT-PilU to generate the high retraction forces required for uptake of chitin-adsorbed tDNA. Consistent with this, *pilT^{R35E}* did not impact NT when tDNA was freely soluble (**Fig. 4a**), suggesting that PilT-PilU$^{C\text{-}term}$ contacts are specifically required for forceful T4P retraction. Together, these results suggest that PilT-PilU$^{C\text{-}term}$ contacts are critical for these motors to coordinate under physiologically relevant conditions where forceful T4P retraction is necessary for DNA uptake.

While these data suggest that PilT-PilU$^{C\text{-term}}$ contacts are important for high force retraction, it remains unclear why coordination between PilT and PilU is necessary to generate high retraction forces. Our results thus far indicate that PilT-PilU form stacked hexamers that are arranged head-to-tail, and that PilU$^{C\text{-term}}$ binds to the sides of the PilT hexamer in a manner that could allow PilU to "pull" on PilT during its catalytic cycle. It is possible this arrangement allows these motors to intimately coordinate their catalytic cycles to combine their efforts and generate forces that could not be achieved by either motor alone. To explore this idea, we sought to estimate the maximum force that a single T4P retraction ATPase can generate (see **Methods** for details). This estimate is derived from four main assumptions: 1) that the free energy of ATP hydrolysis under physiological conditions is -47 kJ/mol (34), 2) that two molecules of ATP are hydrolyzed per catalytic cycle (12, 35), 3) that each catalytic cycle removes one pilin subunit from the pilus filament resulting in a step size of 1 nm (13, 36), and 4) that AAA+ motor ATPases like PilT/PilU operate at an efficiency of ~32.5% (37, 38). Based on this, we estimate that a single T4P retraction motor can generate ~50 pN of force. T4P, however, have empirically been shown to retract at forces that exceed 100 pN (39-41). Thus, molecular coordination between PilT-PilU may, in fact, be necessary to achieve the high T4P retraction forces observed in nature.

According to this model, the ATPase activity of both PilT and PilU should be necessary to generate high retraction forces. To test this, we assessed the transformation of strains where the ATPase activity of either PilT or PilU is ablated via a Walker A mutation (*pilU*^{WA} and *pilT*^{WA}) in chitin flow biofilms where high force retraction is required for DNA uptake. Consistent with our model, both *pilT*^{WA} and *pilU*^{WA} had reduced transformation frequencies compared to the parent when the tDNA was adsorbed to the chitin (**Fig. 4b-c**). Importantly, transformation was indistinguishable from the parent when the tDNA was freely soluble (**Fig. 4a**). Together, these data suggest that the ATPase activity of both PilT and PilU is required for maximal T4P retraction force. Interestingly, *pilU*^{WA} did not phenocopy the transformation deficit of Δ*pilU* in these assays (**Fig. 4b-c**). This may suggest that PilU can also promote forceful retraction in a manner that is independent of its ATPase activity (see **Discussion**).

PilT-PilU$^{C\text{-term}}$ contacts are important for T4P retraction in Acinetobacter baylyi

PilU is broadly conserved among gammaproteobacteria including, but not limited to, *Acinetobacter baylyi*, *Pseudomonas aeruginosa*, *Legionella pneumophila*, and *Xylella fastidiosa* (**Fig. S5a**). Thus, we next sought to determine whether PilT-PilU$^{C\text{-term}}$ contacts are a conserved mechanism for PilT-PilU coordination in diverse T4P systems. Sequence alignments highlight that while the majority of PilU$^{C\text{-term}}$ is not conserved, the PilU$_{Vc}^{K348}$ residue that forms a salt bridge with PilT$_{Vc}^{D2,E53}$ is conserved in all PilU homologs (**Fig. S5a**). Accordingly, the PilT$_{Vc}^{D2,E53}$-PilU$_{Vc}^{K348}$ salt bridge is conserved in AF3 predictions of these PilT-PilU homologs (**Fig. S5b**).

Acinetobacter baylyi competence T4P represent another well-established model system for studying T4P (18, 25, 42-45). For this T4P system, NT is also a simple and sensitive readout (~4-logs of dynamic range) for pilus retraction (**Fig. 5b**). In addition, prior work demonstrates that

351 *pilU$_{Ab}$* is critical for T4P retraction in a *pilT$_{Ab}^{WA}$* background (18), a finding that we recapitulate
352 here (**Fig. 5b**).
353
354 The PilT$_{Ab}^{D2,D53}$-PilU$_{Ab}^{K351}$ contact in *A. baylyi* (**Fig. 5a**) is equivalent to the PilT$_{Vc}^{D2,E53}$-PilU$_{Vc}^{K348}$
355 salt bridge that facilitates PilT-PilU-dependent retraction in *V. cholerae* (**Fig. S5a-b**). To test
356 whether PilT-PilU$^{C\text{-term}}$ contacts are also required for the coordination of these motor ATPases in
357 *A. baylyi*, we targeted the PilT$_{Ab}^{D2,D53}$-PilU$_{Ab}^{K351}$ interface for mutational analysis. Flipping the
358 charge on either side of the interface (*pilT^{WA,D2K,D53R} pilU^{WT}* or *pilT^{WA} pilU^{K351D}*) results in an NT
359 deficit that is indistinguishable from *pilT^{WA}* Δ*pilU* (**Fig. 5b**). Importantly, *pilT^{D2K,D53R}* did not
360 impact PilT-dependent retraction (**Fig. 5b**; compare *pilT^{D2K,D53R}* Δ*pilU* to *ΔpilU*), and steady-state
361 levels of PilU^{K351D} were similar to the PilU^{WT} parent (**Fig. S7b)**. Flipping the charge on both sides
362 of the interface (*pilT^{WA,D2K,}*^{D53R} *pilU^{K351D}*) partially (~1.5-log) restores NT (**Fig. 5b**), which strongly
363 suggests that these residues form a salt bridge. Together, these results indicate that PilT-PilU^{C-}
364 ^{term} contacts are a conserved mechanism for PilT-PilU coordination in diverse T4P.
365
366
367 **DISCUSSION**
368 While prior work established that PilU requires PilT to facilitate retraction (18, 19), a molecular
369 explanation for this interdependence was lacking. Here, we show that PilT is required to
370 "bridge" PilU interactions with the T4P machine *in vivo*. By contrast, PilT could engage T4P
371 machines even in the absence of PilU. PilT homologs contain a highly conserved "AIRNLIRE"
372 motif at the C-terminus (**Fig. S5a**) (46). The PilT-PilC AF3 model places the AIRNLIRE motif within
373 the PilT-PilC interface (**Fig. S11**)(47), suggesting that it may be required for PilT-PilC interactions.
374 Interestingly, the AIRNLIRE motif is not conserved among PilU homologs (**Fig. S5**), which may be
375 one reason why PilU does not directly engage the PilC platform. Our results also provide insight
376 into *how* PilT and PilU interact to coordinate retraction. Specifically, we show that interactions
377 between PilT and the PilU$^{C\text{-term}}$, a feature that is unique to PilU homologs (**Fig. S5a**), is critical for
378 these proteins to promote T4P retraction. The strong conservation between PilT and PilU
379 indicates that PilU likely arose through duplication of PilT and subsequent evolution of the
380 resulting paralog (12, 48). Thus, it is tempting to speculate that the emergence of PilT-PilU
381 coordination required loss of the "AIRNLIRE" motif and gain of the C-terminal extension in PilU.
382
383 While our results show that PilT-PilU$^{C\text{-term}}$ interactions are critical for motor coordination, it is
384 important to acknowledge that this is likely only one of the many molecular interactions that
385 are required for these motors to coordinate. Prior work demonstrates that T4P motor ATPases
386 likely adopt a C2 symmetry and undergo dynamic conformational changes throughout their
387 catalytic cycle (12, 35, 49). AF3, however, only models PilT and PilU with C6 symmetry,
388 highlighting that these models cannot provide insight into the molecular interactions required
389 for motor coordination throughout the PilT-PilU catalytic cycle. Future work will focus on
390 integrating the catalytic dynamics of these motor proteins with the PilT-PilU$^{C\text{-term}}$ interactions
391 identified in our study.
392
393 Although our results provide insight into the molecular coordination between PilT-PilU, it
394 remains unclear why this coordination is necessary. Here, we propose a model where

395 coordination of the catalytic cycles of both PilT and PilU is necessary to generate the high T4P
396 retraction forces observed in nature. Consistent with this, we show that the ATPase activity of
397 both PilT and PilU contributes to tDNA uptake in conditions that require forceful retraction.
398 Interestingly, our results suggest that PilU may promote forceful T4P retraction in multiple ways:
399 1) in an ATPase-dependent manner (**Fig. 4b**; compare parent to *pilU*^{WA}) and 2) in an ATPase-
400 independent manner (**Fig. 4b**; compare *pilU*^{WA} to Δ*pilU*). One explanation for this ATPase-
401 independent effect is that PilU allosterically stimulates PilT activity (*e.g.*, by increasing the
402 mechanical work output of PilT's ATPase cycle to enhance its efficiency). This hypothesis,
403 however, is challenging to test empirically because purified PilT and PilU have no detectable
404 ATPase activity *in vitro* (18), which may suggest that motor-T4P machine interactions are
405 required for ATPase activity.
406
407 Motor ATPase coordination is a prevalent feature among diverse T4P systems. Several
408 gammaproteobacteria encode PilT and PilU homologs (**Fig. S5**), and we demonstrate that the
409 broadly conserved PilT^{D2,E53}-PilU^{K348} salt bridge is important for PilT-PilU coordination in both *V.*
410 *cholerae* and *A. baylyi*. While PilT^{R35} and PilT^{K36} are also conserved among PilT homologs (**Fig.**
411 **S5a**), the specific contacts between these residues and PilU are not conserved; in fact, the C-
412 terminal region of PilU past K348 is poorly conserved (**Fig. S5a**). This suggests that PilT-PilU
413 coordination may be mediated by both conserved and species-specific PilT-PilU$^{C\text{-term}}$
414 interactions. Consistent with this, PilU homologs from different species cross-complement with
415 varying degrees of efficacy (26). Outside of the gammaproteobacteria, some species encode
416 multiple PilT paralogs (*e.g.*, *Neisseria spp.* and *Myxococcus spp.*), suggesting that motor ATPase
417 coordination may also be conserved in more distantly related T4P systems. Additionally, some
418 T4P rely on multiple motor ATPases for pilus extension (42, 50), suggesting that motor
419 coordination may be a critical feature of both T4P extension and retraction.
420
421
422 **METHODS**
423 ***Bacterial strains and culture conditions***
424 *Vibrio cholerae* and *Acinetobacter baylyi* strains were routinely grown in LB broth and on LB
425 agar plates. Medium was supplemented with kanamycin (50 µg/mL), spectinomycin (200
426 µg/mL), sulfamethoxazole (100 µg/mL), trimethoprim (10 µg/mL), carbenicillin (100 µg/mL),
427 and chloramphenicol (1 µg/mL) when appropriate. A comprehensive list of strains used in this
428 study can be found in **Table S1**.
429
430 ***Natural Transformation (NT) assays***
431 Chitin-independent NT assays of *V. cholerae* were conducted using strains where 1) TfoX, the
432 master competence regulator, was placed under an IPTG-inducible promoter (P_{tac}-*tfoX*), and 2)
433 *luxO* was deleted to genetically lock cells in a high-density state. To induce natural competence,
434 strains were grown to late-log by rolling at 30 °C in LB supplemented with 20 mM $MgCl_2$, 10 mM
435 $CaCl_2$, and 100 µM IPTG. Then, 7 µL of this culture was diluted into 350 *µL* of Instant Ocean
436 medium (IO; 7 g/L Aquarium Systems) for each transformation reaction. Two reactions were
437 setup for each strain: one where 100 ng of tDNA (a ΔVC1807::Kan^R PCR product) was added and
438 a negative control where no tDNA was added. After 3 min of tDNA incubation, 6 units of DNase I

439 (NEB) was added to stop DNA uptake, and reactions were incubated overnight at 30 °C to allow
440 for tDNA integration. The next day, 0.5 mL LB was added, and reactions were outgrown at 37 °C
441 shaking for 3 hrs. Reactions were then dribble plated for quantitative culture on LB plates with
442 kanamycin (to quantify transformant CFUs) and on plain LB agar plates (to quantify total CFUs).
443 The transformation frequency was determined by dividing the CFUs of transformants by the
444 total CFUs. For reactions with no transformants, the limit of detection was calculated and
445 plotted.
446
447 Chitin-dependent NT assays of *V. cholerae* in the presence of soluble DNA or chitin adsorbed
448 DNA were conducted exactly as previously described (24). Briefly, strains contained two
449 fluorescent reporters: a disrupted GFP construct (ΔVC1807::Cm^R-*lacI*-P_{tac}-*gfp::parST1*) and a
450 constitutively expressed mKate2 construct (Δ*lacZ*::$Spec^R$-*lacI*-P_{tac}-*mKate2*).
451 For assays where free DNA was supplied, strains were grown rolling at 30 °C in LB to
452 mid-log. Cells were then washed and adjusted to an OD_{600} = 1.0 in IO. Next, chitin-dependent
453 transformation reactions were setup by mixing the following in a 2mL eppi: 100 µL of cells, 150
454 µL chitin slurry (8 g / 150 mL IO; Alfa Aesar), and 750 µL IO. Two reactions were prepped for
455 each strain. Reactions were incubated static overnight at 30 °C to induce natural competence.
456 The next day, 1000 ng of tDNA (a ΔVC1807::Cm^R-*lacI*-P_{tac}-*gfp* PCR product) was added to one
457 reaction, while no DNA was added to the other reaction, which served as a negative control. All
458 reactions were incubated overnight at 30 °C with shaking to ensure the tDNA remained in
459 solution. The next day, cells were harvested from the chitin, placed under a 0.4% IO gelzan pad
460 and imaged via epifluorescence microscopy with FITC and mCherry filter cubes. Images were
461 analyzed using MicrobeJ to determine the number of mKate (total) and GFP (transformant)
462 fluorescent cells. Transformation frequency was calculated by dividing the GFP (transformant)
463 cell counts by the mKate (total) cell counts (at least 500 cells analyzed in each sample).
464 For assays where tDNA was chitin adsorbed, flow cells (24) containing chitin flakes were
465 first washed with 0.13 ng/µL of tDNA (a ΔVC1807::Cm^R-*lacI*-P_{tac}-*gfp* PCR product) at a
466 volumetric flow rate of 0.1 µL/min for 24 h. Following this tDNA adsorption step, the flow cell
467 inlet tubing was swapped to blank defined artificial seawater (DASW; consists of 234 mM NaCl,
468 27.5 mM MgSO4, 1.5 mM NaHCO3, 4.95 mM CaCl2, 5.15 mM KCl, 0.07 mM Na2B4O7, 0.05 mM
469 SrCl, 0.015 mM NaBr, 0.001 mM NaI, 0.013 mM LiCl, 0.187 mM K2HPO4, and pH 7.1
470 triethanolamine) and flow was maintained at 0.1 µL/min for an additional 24 h to remove any
471 unbound tDNA. After this wash step, 100 µL of reporter cells were resuspended in DASW to an
472 OD_{600} of 5.0 and inoculated into the chambers via syringe, after which flow with blank DASW
473 was resumed. The reporter strain was then incubated at room temperature (~22 °C) for 48 h
474 before imaging. Flow cells were imaged using a Zeiss 880 line-scanning confocal microscope and
475 a 40x/1.2 N.A. water objective. A 488 nm laser line was used to excite the GFP protein
476 expressed after transformation events and a 594 nm laser line was used to excite the mKate2
477 protein carried by the reporter strain. BiofilmQ was used to threshold images and quantify the
478 reporter (mKate2 labeled) and transformant (GFP labeled) biovolumes (51). The transformation
479 frequency was calculated as GFP biovolume divided by mKate2 biovolume. For samples where
480 no transformants were observed, the approximate biovolume of a single cell was used to
481 calculate the limit of detection and plotted.
482

483 For NT assays of *A. baylyi*, overnight cultures were washed and adjusted to an OD_{600} = 2.0 in
484 fresh LB. Then, 50 µL of this culture was added to 450 µL LB supplemented with 20 mM $MgCl_2$
485 and 10 mM $CaCl_2$ in a 2 mL eppi. Two transformation reactions were setup for each strain: one
486 where 50 ng of tDNA (a ΔACIAD1551::Kan^R PCR product) was added and a negative control
487 where no tDNA was added. Transformations were incubated with end-over-end rotation at 30
488 °C for 45 mins. After 45 min of tDNA incubation, 6 units of DNase I (NEB) was added to stop
489 DNA uptake, and reactions were incubated with end-over-end rotation at 30 °C for an additional
490 5 hrs to allow for tDNA integration and outgrowth. Reactions were then dribble plated for
491 quantitative culture on LB plates with kanamycin (to quantify transformant CFUs) and on plain
492 LB agar plates (to quantify total CFUs). The transformation frequency was determined by
493 dividing the CFUs of transformants by the total CFUs. For reactions with no transformants, the
494 limit of detection was calculated and plotted.
495
496 ***Construction of mutant strains***
497 All *V. cholerae* strains used in this study were derivatives of the El Tor isolate E7946 (52). All *A.*
498 *baylyi* strains were derivatives of strain ADP1 (53). All mutant strains were generated by NT (as
499 described above). Mutant constructs were generated by splicing-by-overlap-extension (SOE)
500 exactly as previously described (54-56). A list of all primers used to generate mutant constructs
501 can be found in **Table S2**.
502
503 ***Microscopy***
504 Unless otherwise indicated, phase and epifluorescence (FITC, YFP, mCherry channels) images
505 were collected on an inverted Nikon Ti-2 microscope with a Plan Apo ×60 objective fitted with a
506 Hamamatsu ORCAFlash 4.0 camera using Nikon NIS Elements imaging software.
507
508 ***Motor localization assay***
509 For these assays, all *V. cholerae* strains contained the P_{tac}-*tfoX* and Δ*luxO* mutations required for
510 chitin-independent induction of competence as describe above for NT assays. Cells were grown
511 overnight in LB supplemented with 20 mM $MgCl_2$, 10 mM $CaCl_2$, and 100 µM IPTG rolling at 30
512 °C. The next day, 500 µL of overnight culture was subcultured into 3 mL of LB supplemented
513 with 20 mM $MgCl_2$, 10 mM $CaCl_2$, and 100 µM IPTG and grown for 1 hr rolling at 30 °C. Then,
514 100 µL of this culture was spun down and washed in IO. Cells were then placed under a 0.4% IO
515 gelzan pad and imaged via timelapse microscopy (2 sec intervals for 10 sec duration) with the
516 phase contrast and mCherry channels. Quantification of fluorescent foci was performed using
517 MicrobeJ features detection. Foci were only counted if they moved less than 0.3 µm between
518 frames and were present in all frames of the timelapse.
519
520 For quantification of colocalizing foci, cells were imaged via timelapse microscopy (2 sec
521 intervals for 10 sec duration) with the phase contrast, FITC, and mCherry channels. For
522 colocalizing PilT and PilU foci, MicrobeJ features detection was used to identify cells with GFP-
523 PilU foci. Then, the presence of a colocalizing PilT-mCherry focus was determined manually. The
524 results are presented as the percentage of GFP-PilU foci that colocalized with mCherry-PilT foci.
525 For motor and PilQ foci, the MicrobeJ colocalization feature was used to identify colocalizing

526 motor and msfGFP-PilQ foci that were less than 0.4 µm apart. Results are presented as the
527 percentage of motor foci that colocalized with msfGFP-PilQ foci.
528
529 ***Pilus labeling and imaging***
530 *V. cholerae* strains were grown exactly as described above for chitin-independent NT assays.
531 Then, 100 µL of late-log cells were pelleted at 8000 x g for 1 min and washed in IO. Cells were
532 then labeled with 25 µg/mL AF488-mal for 15 mins static at room temperature. Cells were then
533 washed three times in IO, ensuring to spin at 8000 x g for 1 min to prevent shearing of surface
534 pili. Cells were then placed under a 0.4% IO gelzan pad and imaged with the phase and FITC
535 channels. Representative images of the piliation phenotype for each strain were selected from
536 the raw microscopy images.
537
538 ***T4P-dependent aggregation assay***
539 *V. cholerae* strains were grown exactly as described above for chitin-independent NT assays.
540 Subcultures were allowed to sit static at room temperature on the benchtop for 15 mins to let
541 cellular aggregates settle out of solution. Representative images were taken of each strain
542 without disturbing settled cells.
543
544 ***AF3-MD analysis***
545 The initial structure of the PilT-PilU complex was generated using AlphaFold 3 (28). Propka3 was
546 used to assign the charges of the ionizable residues and the protonation state of histidine
547 residues (57). $PilU^{D253}$ and $PilU^{E280}$ were protonated. Based on their local electrostatic
548 environment, $PilT^{H151}$, $PilT^{H166}$, $PilT^{H183}$, $PilT^{H229}$, $PilT^{H280}$, $PilU^{H164}$, $PilU^{H240}$, and $PilU^{H276}$ were set
549 to HSE (histidine-epsilon). All other histidine residues were set to HSD (histidine-delta).
550
551 The PilT-PilU structure was subsequently solvated, using CHARMM-GUI, v3.7 generating a 162$Å^3$
552 water box (58, 59). Potassium (K^+) and chloride (Cl^-) ions were added in order to neutralize the
553 system as well as produce an ionic strength of 150 mM. Simulations were conducted with
554 NAMD3 (60) using the CHARMM36m protein force field (61), and TIP3P water model (62). The
555 initial structure was minimized for 10,000 steps, followed by a two-stage equilibration: first, 1ns
556 of MD was run while restraining the protein heavy atoms, and second, 4ns of MD was run while
557 restraining only the protein backbones, thereby equilibrating the box dimensions. Production
558 runs were performed using hydrogen mass repartitioning (HMR), allowing for a uniform 4 fs
559 time step (63, 64).
560
561 The simulations were run at a constant temperature (310 K) and constant isotropic pressure (1
562 atm), maintained by a Langevin thermostat and piston, respectively (65). Long-range
563 electrostatics were calculated at every time step using the particle-mesh Ewald method (66).
564 We set a short-range cutoff for Lennard-Jones interactions at 12 Å with a switching function
565 starting at 10 Å. Two independent replicas were performed for 500 ns.
566
567 Animations were rendered with VMD v1.9.4a51 (67), and the distance calculations were
568 performed with MDAnalysis (68, 69), where the minimum distance between two residue side
569 chains was taken as the closest pair of heavy atoms. In the case where multiple interactions are

570 considered (e.g. PilT^{R35}-PilU^{D366,E368}), the minimum distance was taken for either residue in the
571 target pair. Salt bridges and contacts were defined when this distance was less than a cutoff of
572 3.5 Å or 4.5 Å, respectively.
573
574 Simulations of the PilT-PilU^{D366K} AF3 complex were performed as described above except the
575 number of positive ions was adjusted to ensure neutrality of the simulation cell.
576
577 ***Estimating T4P force generation***
578 The following equation was used to calculate the maximal force (F_{max}) generated by a T4P
579 motor ATPase:

580 $$F_{max} = \frac{Energy\ consumed\ (J)}{Step\ size\ (m)}$$

581
582 The energy consumed was determined based on two assumptions: 1) the free energy of ATP
583 hydrolysis in physiological conditions is -47 kJ/mol (34) and 2) that two molecules of ATP are
584 hydrolyzed per ATPase cycle (12, 35). Based on this, the free energy released upon hydrolysis of
585 two ATP molecules was determined to be 1.56 x 10^{-19} J. To estimate the step size, we assumed
586 that one pilin is removed from the pilus filament in each ATPase cycle resulting in a step size of 1
587 nm (or 1 x 10^{-9} m) (13, 36). These values were then plugged into the equation above to calculate
588 the F_{max} generated by T4P motors at 100% efficiency:
589

590 $$F_{max} = \frac{1.56 \text{ x } 10^{-19} \text{ J}}{1 \text{ x } 10^{-9}\ m} = 1.56 \text{ x } 10^{-10}\ N = 156 \text{ pN}$$

591
592 It is unlikely that these motor proteins operate at 100% efficiency. Prior work has defined the
593 efficiencies of two other members of the AAA+ family of motor ATPases: the phi29 packing
594 motor = 30% (37) and ClpX = 35% (38). We averaged these values (32.5%) to generate an
595 estimate for the efficiency of this family of motor ATPases. Accounting for average efficiency, we
596 estimated that a single T4P motor can maximally generate ~50.7 pN of force.
597
598 ***Generating multiple sequence alignments***
599 Multiple sequence alignments (MSA) were generated by first gathering the PilT and PilU protein
600 sequences from each organism from GenBank. Sequences were then aligned using T-Coffee
601 (70), and the alignments were reformatted for the final figure using the Sequence Manipulation
602 Suite: Color Align Conservation tool (71).
603
604 ***Western blotting***
605 Strains of *V. cholerae* and *A. baylyi* were grown exactly as described above for natural
606 transformation assays for each respective organism. Cultures were then washed and
607 resuspended to an OD_{600} = 100 in IO. Cells were mixed 1:1 with 2x SDS-PAGE sample buffer
608 (200 mM Tris pH 6.8, 25% glycerol, 4.1% SDS, 0.02% Bromophenol Blue, 5% β-mercaptoethanol)
609 and boiled at 100°C for 10 mins. To blot for 3xFLAG-PilU or RpoA, 2 µL of each sample was
610 electrophoretically separated on 10% SDS-PAGE gels. Following SDS-PAGE, the proteins were
611 transferred to a polyvinylidene difluoride (PVDF) membrane by electrophoresis. Next, the

membranes were blocked with 5% milk solution for 1 hr rocking at room temperature. To blot for 3xFLAG-pilU, primary mouse monoclonal anti-FLAG M2 antibody was added to the membrane. To blot for RpoA, primary mouse monoclonal anti-RpoA antibody was added, and membranes were incubated rocking at room temperature overnight. The next day, membranes were washed and incubated with anti-mouse horseradish peroxidase-conjugated secondary antibody for two hours rocking at room temperature. Lastly, blots were washed, developed with Pierce ECL Western blotting substrate, and imaged with a ProteinSimple FluorChem R system.

Summary Statistics

See **Dataset S1** for summary statistics and a comprehensive list of statistical comparisons for all quantitative data in this manuscript.

ACKNOLWEDGEMENTS

We would like to thank Marc Morais for helpful discussions. This work was supported by grant R35GM128674 from the National Institutes of Health (NIH) to ABD and R01GM148586 from NIH to JCG.

REFERENCES

1. P. Seitz, M. Blokesch, DNA-uptake machinery of naturally competent Vibrio cholerae. *Proc Natl Acad Sci U S A* **110**, 17987–17992 (2013).
2. C. Pujol, E. Eugene, M. Marceau, X. Nassif, The meningococcal PilT protein is required for induction of intimate attachment to epithelial cells following pilus-mediated adhesion. *Proc Natl Acad Sci U S A* **96**, 4017–4022 (1999).
3. C. K. Ellison *et al.*, Obstruction of pilus retraction stimulates bacterial surface sensing. *Science* **358**, 535–538 (2017).
4. A. J. Merz, M. So, M. P. Sheetz, Pilus retraction powers bacterial twitching motility. *Nature* **407**, 98–102 (2000).
5. J. M. Skerker, H. C. Berg, Direct observation of extension and retraction of type IV pili. *Proc Natl Acad Sci U S A* **98**, 6901–6904 (2001).
6. I. Guilvout *et al.*, Membrane platform protein PulF of the Klebsiella type II secretion system forms a trimeric ion channel essential for endopilus assembly and protein secretion. *mBio* **15**, e0142323 (2024).
7. M. McCallum, S. Tammam, J. L. Rubinstein, L. L. Burrows, P. L. Howell, CryoEM map of Pseudomonas aeruginosa PilQ enables structural characterization of TsaP. *Structure* **29**, 457–466 e454 (2021).
8. Y. W. Chang *et al.*, Architecture of the type IVa pilus machine. *Science* **351**, aad2001 (2016).
9. S. J. Weaver *et al.*, CryoEM structure of the type IVa pilus secretin required for natural competence in Vibrio cholerae. *Nat Commun* **11**, 5080 (2020).
10. M. Wolfgang, J. P. van Putten, S. F. Hayes, D. Dorward, M. Koomey, Components and dynamics of fiber formation define a ubiquitous biogenesis pathway for bacterial pili. *EMBO J* **19**, 6408–6418 (2000).
11. C. K. Ellison *et al.*, Retraction of DNA-bound type IV competence pili initiates DNA uptake during natural transformation in Vibrio cholerae. *Nat Microbiol* **3**, 773–780 (2018).
12. M. McCallum, S. Tammam, A. Khan, L. L. Burrows, P. L. Howell, The molecular mechanism of the type IVa pilus motors. *Nat Commun* **8**, 15091 (2017).
13. L. Craig *et al.*, Type IV pilus structure by cryo-electron microscopy and crystallography: implications for pilus assembly and functions. *Mol Cell* **23**, 651–662 (2006).

14. C. B. Whitchurch, M. Hobbs, S. P. Livingston, V. Krishnapillai, J. S. Mattick, Characterisation of a Pseudomonas aeruginosa twitching motility gene and evidence for a specialised protein export system widespread in eubacteria. *Gene* **101**, 33–44 (1991).
15. M. Wolfgang, H. S. Park, S. F. Hayes, J. P. van Putten, M. Koomey, Suppression of an absolute defect in type IV pilus biogenesis by loss-of-function mutations in pilT, a twitching motility gene in Neisseria gonorrhoeae. *Proc Natl Acad Sci U S A* **95**, 14973–14978 (1998).
16. H. S. Park, M. Wolfgang, M. Koomey, Modification of type IV pilus-associated epithelial cell adherence and multicellular behavior by the PilU protein of Neisseria gonorrhoeae. *Infect Immun* **70**, 3891–3903 (2002).
17. C. B. Whitchurch, J. S. Mattick, Characterization of a gene, pilU, required for twitching motility but not phage sensitivity in Pseudomonas aeruginosa. *Mol Microbiol* **13**, 1079–1091 (1994).
18. J. L. Chlebek *et al.*, PilT and PilU are homohexameric ATPases that coordinate to retract type IVa pili. *PLoS Genet* **15**, e1008448 (2019).
19. D. W. Adams, J. M. Pereira, C. Stoudmann, S. Stutzmann, M. Blokesch, The type IV pilus protein PilU functions as a PilT-dependent retraction ATPase. *PLoS Genet* **15**, e1008393 (2019).
20. J. Thongchol *et al.*, Removal of Pseudomonas type IV pili by a small RNA virus. *Science* **384**, eadl0635 (2024).
21. P. Seitz *et al.*, ComEA is essential for the transfer of external DNA into the periplasm in naturally transformable Vibrio cholerae cells. *PLoS Genet* **10**, e1004066 (2014).
22. A. B. Dalia, T. N. Dalia, Spatiotemporal Analysis of DNA Integration during Natural Transformation Reveals a Mode of Nongenetic Inheritance in Bacteria. *Cell* **179**, 1499–1511 e1410 (2019).
23. K. L. Meibom, M. Blokesch, N. A. Dolganov, C. Y. Wu, G. K. Schoolnik, Chitin induces natural competence in Vibrio cholerae. *Science* **310**, 1824–1827 (2005).
24. J. D. Holt, Y. Peng, T. N. Dalia, A. B. Dalia, C. D. Nadell, Environmental DNA adsorption to chitin can promote horizontal gene transfer by natural transformation. *Proc Natl Acad Sci U S A* **122**, e2420708122 (2025).
25. J. L. Chlebek, R. Denise, L. Craig, A. B. Dalia, Motor-independent retraction of type IV pili is governed by an inherent property of the pilus filament. *Proc Natl Acad Sci U S A* **118** (2021).
26. E. Couser, J. L. Chlebek, A. B. Dalia, Retraction ATPase Motors from Three Orthologous Type IVa Pilus Systems Support Promiscuous Retraction of the Vibrio cholerae Competence Pilus. *J Bacteriol* **204**, e0012622 (2022).
27. D. W. Adams, S. Stutzmann, C. Stoudmann, M. Blokesch, DNA-uptake pili of Vibrio cholerae are required for chitin colonization and capable of kin recognition via sequence-specific self-interaction. *Nat Microbiol* 10.1038/s41564-019-0479-5 (2019).
28. J. Abramson *et al.*, Accurate structure prediction of biomolecular interactions with AlphaFold 3. *Nature* **630**, 493–500 (2024).
29. P. Chiang *et al.*, Functional role of conserved residues in the characteristic secretion NTPase motifs of the Pseudomonas aeruginosa type IV pilus motor proteins PilB, PilT and PilU. *Microbiology (Reading)* **154**, 114–126 (2008).
30. K. A. Floyd *et al.*, c-di-GMP modulates type IV MSHA pilus retraction and surface attachment in Vibrio cholerae. *Nat Commun* **11**, 1549 (2020).
31. H. Q. Hughes *et al.*, Nitric oxide stimulates type IV MSHA pilus retraction in Vibrio cholerae via activation of the phosphodiesterase CdpA. *Proc Natl Acad Sci U S A* **119** (2022).
32. S. Maggi *et al.*, Integrative Structure and Function of the Vibrio cholerae Competence Pilus Machine. *bioRxiv* 10.1101/2025.10.14.680967 (2025).
33. C. K. Ellison, T. N. Dalia, A. B. Dalia, Y. V. Brun, Real-time microscopy and physical perturbation of bacterial pili using maleimide-conjugated molecules. *Nat Protoc* **14**, 1803–1819 (2019).
34. Q. H. Tran, G. Unden, Changes in the proton potential and the cellular energetics of Escherichia coli during growth by aerobic and anaerobic respiration or by fermentation. *Eur J Biochem* **251**, 538–543 (1998).
35. M. McCallum *et al.*, Multiple conformations facilitate PilT function in the type IV pilus. *Nat Commun* **10**, 5198 (2019).
36. H. Ochner *et al.*, Structure of the Pseudomonas aeruginosa PAO1 Type IV pilus. *PLoS Pathog* **20**, e1012773 (2024).

37. D. E. Smith *et al.*, The bacteriophage straight phi29 portal motor can package DNA against a large internal force. *Nature* **413**, 748–752 (2001).
38. R. A. Maillard *et al.*, ClpX(P) generates mechanical force to unfold and translocate its protein substrates. *Cell* **145**, 459–469 (2011).
39. B. Maier *et al.*, Single pilus motor forces exceed 100 pN. *Proc Natl Acad Sci U S A* **99**, 16012–16017 (2002).
40. M. Clausen, V. Jakovljevic, L. Sogaard-Andersen, B. Maier, High-force generation is a conserved property of type IV pilus systems. *J Bacteriol* **191**, 4633–4638 (2009).
41. M. D. Koch, M. E. Black, E. Han, J. W. Shaevitz, Z. Gitai, Pseudomonas aeruginosa distinguishes surfaces by stiffness using retraction of type IV pili. *Proc Natl Acad Sci U S A* **119**, e2119434119 (2022).
42. C. K. Ellison *et al.*, Acinetobacter baylyi regulates type IV pilus synthesis by employing two extension motors and a motor protein inhibitor. *Nat Commun* **12**, 3744 (2021).
43. C. K. Ellison *et al.*, Subcellular localization of type IV pili regulates bacterial multicellular development. *Nat Commun* **13**, 6334 (2022).
44. T. J. Ellison, C. K. Ellison, Improved DNA binding to a type IV minor pilin increases natural transformation. *Nucleic Acids Res* **53** (2025).
45. T. J. Ellison, I. Y. Yen, P. L. Howell, C. K. Ellison, FimX regulates type IV pilus localization via the Pil-Chp chemosensory system in Acinetobacter baylyi. *bioRxiv* 10.1101/2025.05.21.655318 (2025).
46. K. G. Aukema, E. M. Kron, T. J. Herdendorf, K. T. Forest, Functional dissection of a conserved motif within the pilus retraction protein PilT. *J Bacteriol* **187**, 611–618 (2005).
47. C. J. Geiger, G. C. L. Wong, G. A. O'Toole, A bacterial sense of touch: T4P retraction motor as a means of surface sensing by Pseudomonas aeruginosa PA14. *J Bacteriol* **206**, e0044223 (2024).
48. R. Denise, S. S. Abby, E. P. C. Rocha, Diversification of the type IV filament superfamily into machines for adhesion, protein secretion, DNA uptake, and motility. *PLoS Biol* **17**, e3000390 (2019).
49. Y. Guo *et al.*, Analysis of the heterogenous structural states of the hexameric ATPase PilU of the Type IV pili from Vibrio cholerae. *bioRxiv* 10.64898/2026.02.06.704419 (2026).
50. H. Q. Hughes, N. D. Christman, T. N. Dalia, C. K. Ellison, A. B. Dalia, The PilT retraction ATPase promotes both extension and retraction of the MSHA type IVa pilus in Vibrio cholerae. *PLoS Genet* **18**, e1010561 (2022).
51. R. Hartmann *et al.*, Quantitative image analysis of microbial communities with BiofilmQ. *Nat Microbiol* **6**, 151–156 (2021).
52. V. L. Miller, V. J. DiRita, J. J. Mekalanos, Identification of toxS, a regulatory gene whose product enhances toxR-mediated activation of the cholera toxin promoter. *J Bacteriol* **171**, 1288–1293 (1989).
53. E. Juni, A. Janik, Transformation of Acinetobacter calco-aceticus (Bacterium anitratum). *J Bacteriol* **98**, 281–288 (1969).
54. A. B. Dalia, Natural Cotransformation and Multiplex Genome Editing by Natural Transformation (MuGENT) of Vibrio cholerae. *Methods Mol Biol* **1839**, 53–64 (2018).
55. A. B. Dalia, E. McDonough, A. Camilli, Multiplex genome editing by natural transformation. *Proc Natl Acad Sci U S A* **111**, 8937–8942 (2014).
56. A. B. Dalia, D. W. Lazinski, A. Camilli, Characterization of undermethylated sites in Vibrio cholerae. *J Bacteriol* **195**, 2389–2399 (2013).
57. M. H. Olsson, C. R. Sondergaard, M. Rostkowski, J. H. Jensen, PROPKA3: Consistent Treatment of Internal and Surface Residues in Empirical pKa Predictions. *J Chem Theory Comput* **7**, 525–537 (2011).
58. S. Jo, T. Kim, V. G. Iyer, W. Im, CHARMM-GUI: a web-based graphical user interface for CHARMM. *J Comput Chem* **29**, 1859–1865 (2008).
59. J. Lee *et al.*, CHARMM-GUI Input Generator for NAMD, GROMACS, AMBER, OpenMM, and CHARMM/OpenMM Simulations Using the CHARMM36 Additive Force Field. *J Chem Theory Comput* **12**, 405–413 (2016).
60. J. C. Phillips *et al.*, Scalable molecular dynamics on CPU and GPU architectures with NAMD. *J Chem Phys* **153**, 044130 (2020).
61. J. Huang *et al.*, CHARMM36m: an improved force field for folded and intrinsically disordered proteins. *Nat Methods* **14**, 71–73 (2017).
62. W. L. Jorgensen, J. Chandrasekhar, J. D. Madura, R. W. Impey, M. L. Klein, Comparison of Simple Potential Functions for Simulating Liquid Water. *Journal of Chemical Physics* **79**, 926–935 (1983).

63. C. W. Hopkins, S. Le Grand, R. C. Walker, A. E. Roitberg, Long-Time-Step Molecular Dynamics through Hydrogen Mass Repartitioning. *J Chem Theory Comput* **11**, 1864–1874 (2015).
64. C. Balusek *et al.*, Accelerating Membrane Simulations with Hydrogen Mass Repartitioning. *J Chem Theory Comput* **15**, 4673–4686 (2019).
65. S. E. Feller, Y. H. Zhang, R. W. Pastor, B. R. Brooks, Constant-Pressure Molecular-Dynamics Simulation - the Langevin Piston Method. *Journal of Chemical Physics* **103**, 4613–4621 (1995).
66. T. Darden, D. York, L. Pedersen, Particle Mesh Ewald - an N.Log(N) Method for Ewald Sums in Large Systems. *Journal of Chemical Physics* **98**, 10089–10092 (1993).
67. W. Humphrey, A. Dalke, K. Schulten, VMD: visual molecular dynamics. *J Mol Graph* **14**, 33–38, 27–38 (1996).
68. N. Michaud-Agrawal, E. J. Denning, T. B. Woolf, O. Beckstein, MDAnalysis: a toolkit for the analysis of molecular dynamics simulations. *J Comput Chem* **32**, 2319–2327 (2011).
69. M. L. R. J. Gowers, J. Barnoud, T. J. E. Reddy, M. N. Melo, S. L. Seyler, D. L. Dotson, J. Domanski, S. Buchoux, I. M. Kenney, and O. Beckstein, MDAnalysis: A Python package for the rapid analysis of molecular dynamics simulations. *Proceedings of the 15th Python in Science Conference* 10.25080/Majora-629e541a-00e, 98–105 (2016).
70. C. Notredame, D. G. Higgins, J. Heringa, T-Coffee: A novel method for fast and accurate multiple sequence alignment. *J Mol Biol* **302**, 205–217 (2000).
71. P. Stothard, The sequence manipulation suite: JavaScript programs for analyzing and formatting protein and DNA sequences. *Biotechniques* **28**, 1102, 1104 (2000).

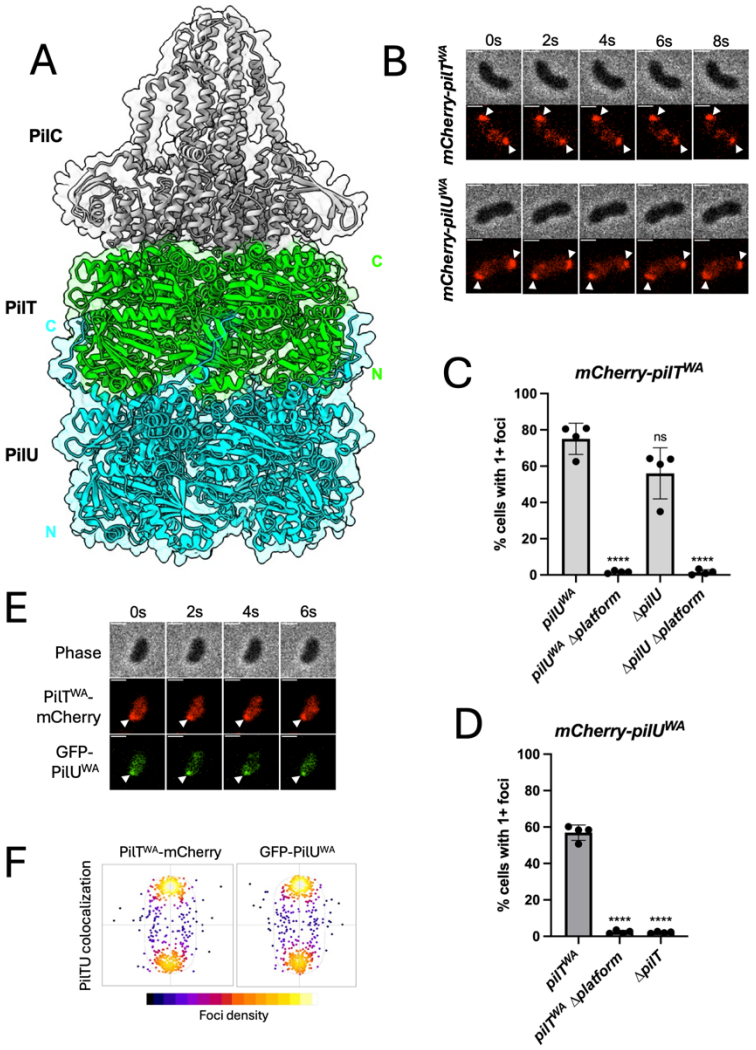

Fig. 1. **PilT bridges PilU to the T4P machine.** (**A**) A hybrid AlphaFold 3 model highlights the putative interactions between PilC (grey), PilT (green), and PilU (cyan). The N-terminal and C-terminal faces of PilT and PilU are labeled with green and cyan letters, respectively. Motor localization assays were performed to assess the localization of PilT and PilU *in vivo* by epifluorescence time lapse microscopy in **B**-**D**. (**B**) Representative montages of timelapse imaging of *V. cholerae* cells expressing mCherry-PilT^{WA} PilU^{WA} and PilT^{WA} mCherry-PilU^{WA} that displayed ATPase foci (white carats). Scale bar, 1 µm. For quantification of these assays, a fluorescent focus was only counted if it was maintained throughout the duration of the 10-s timelapse. (**C**) Motor localization assay of cells expressing *mCherry-pilT^{WA}* (WA = the *pilT^{K136A}* Walker A mutation that ablates ATPase activity) and the indicated mutations. The Δ*platform* mutation denotes a mutant lacking both the competence T4P platform *pilC* and the MSHA T4P platform *mshG*. For each strain, the percentage of cells (n = 120 cells analyzed) with one or more fluorescent mCherry-PilT^{WA} foci is reported. (**D**) Motor localization assay of cells expressing *mCherry-pilU^{WA}* (WA = the *pilU^{K134A}* Walker A mutation that ablates ATPase activity) and the indicated mutations. For each strain, the percentage of cells (n = 120 cells analyzed) with one or more fluorescent mCherry-PilU^{WA} foci is reported. (**E**) Motor localization assay of cells expressing *pilT^{WA}-mCherry gfp-pilU^{WA}*. The representative montage of timelapse imaging shows colocalization of PilT^{WA}-mCherry and GFP-PilU^{WA} (white carat). (**F**) Cell scatter plots show the localization of PilT^{WA}-mCherry and GFP-PilU^{WA} foci in the colocalization strain shown in **E**. Both PilT and PilU foci primarily localize to the cell poles. Data in **C**-**D** are from 4 independent biological replicates and shown as the mean ± SD. Statistical comparisons were made by one-way ANOVA with Tukey's multiple comparison test of the log-transformed data. ns, not significant; **** = $p < 0.0001$. Symbols directly above bars denote comparisons to the appropriate parent strain.

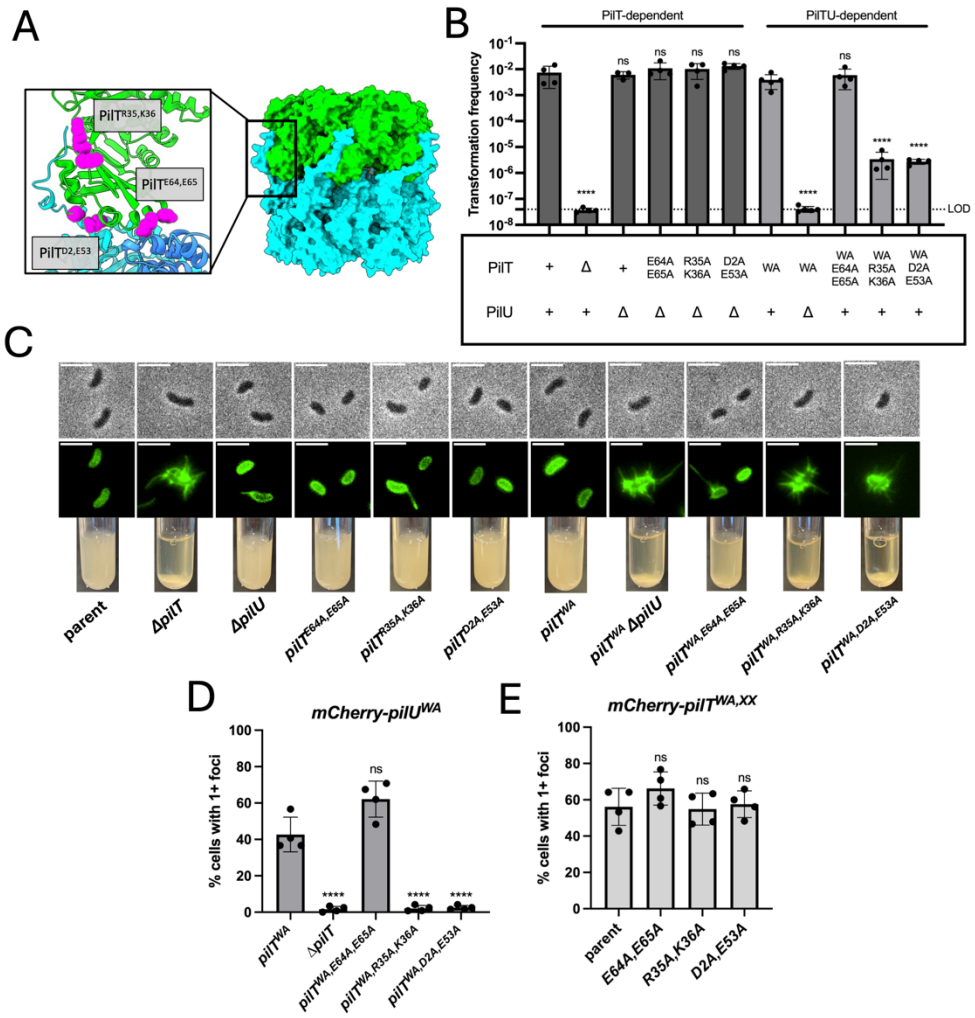

Fig. 2. **Contacts between PilT and the PilU$^{C\text{-term}}$ are critical for PilT-PilU interactions and T4P retraction.** (**A**) AF3 model of PilT (green)-PilU (cyan) interactions. Inset highlights the interaction interfaces targeted for mutagenesis. The PilT residues that putatively participate in intermolecular salt bridges are shown in magenta. (**B**) NT assays of the indicated *V. cholerae* strains. Dark gray bars denote strains that report on PilT-dependent retraction (*i.e.*, in a *pilT*$^{+}$ background where PilT ATPase activity is intact), while light grey bars denote strains that report on PilT-PilU-dependent retraction (*i.e.*, in a *pilT*^{WA} background where retraction is dependent on PilU). LOD, limit of detection. (**C**) Representative images of surface piliation (top panel) and cellular aggregation (bottom panel) for the indicated strains. Scale bars on micrographs, 3 µm. Data are representative of two independent experiments. (**D**) Motor localization assay of cells expressing *mCherry-pilU*^{WA} and the indicated *pilT* alleles. For each strain, the percentage of cells (n = 120 cells analyzed) with one or more fluorescent mCherry-PilU^{WA} foci is reported. (**E**) Motor localization assay of Δ*pilU* cells expressing an *mCherry-pilT*^{WA} construct with the additional mutations indicated. For each strain, the percentage of cells (n = 120 cells analyzed) with one or more fluorescent mCherry-PilT^{WA} foci is reported. Data in **B**, **D**, and **E** are from 4 independent biological replicates and shown as the mean ± SD. Statistical comparisons were made by one-way ANOVA with Tukey's multiple comparison test of the log-transformed data. ns, not significant; **** = $p < 0.0001$. Symbols directly above bars denote comparisons to the appropriate parent strain; in **B**, symbols above the dark grey bars denote comparisons to the parent strain, while symbols above the light grey bars denote comparisons to *pilT*^{WA}.

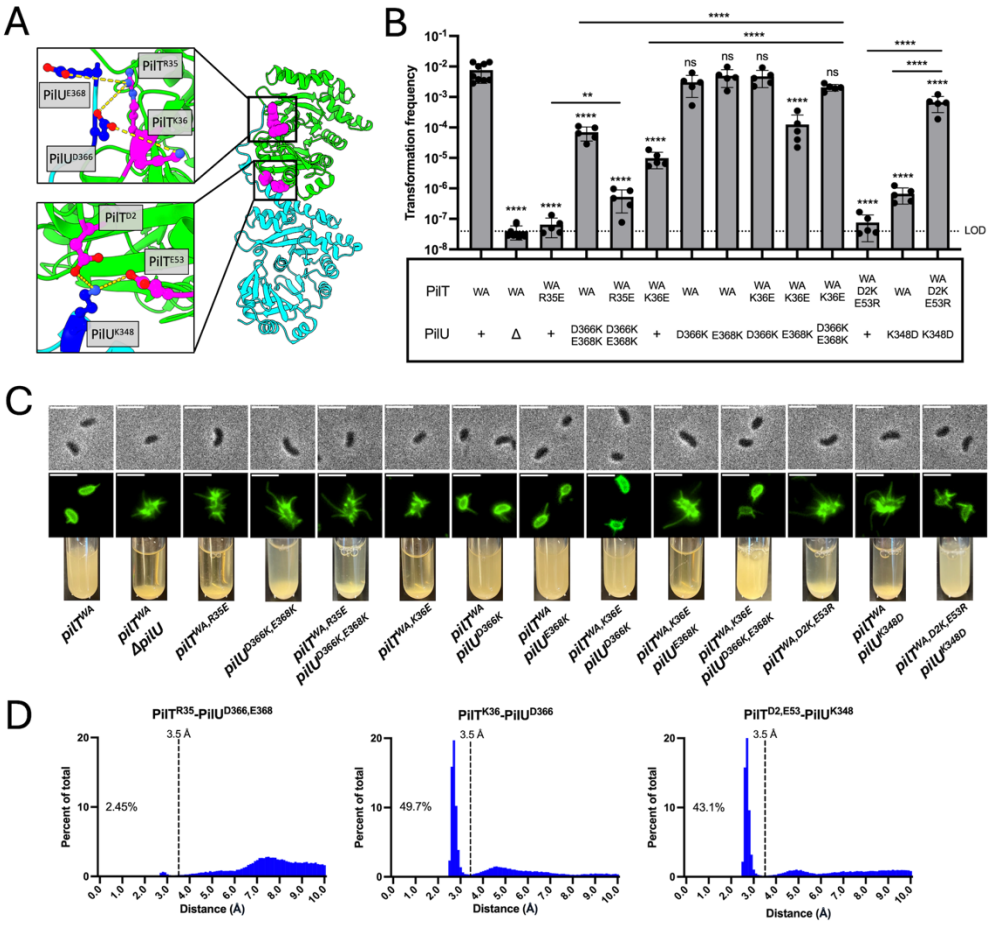

Fig. 3. **AF3-MD simulations and high-resolution genetic analysis reveal PilT-PilU$^{C\text{-}term}$ salt bridges required for motor coordination.** (**A**) AF3 model of PilT (green)-PilU (cyan) interactions. The inset highlights the residues that participate in the three putative salt bridges targeted for mutagenesis. PilT residues are shown in magenta with nitrogen atoms colored blue, and PilU residues are shown in dark blue with oxygen atoms colored red. (**B**) NT assay of the indicated *V. cholerae* strains. Data are from five independent biological replicates and shown as the mean ± SD. LOD, limit of detection. Statistical comparisons were made by one-way ANOVA with Tukey's multiple comparison test of the log-transformed data. ns, not significant; ** = $p < 0.01$; **** = $p < 0.0001$. Symbols directly above bars denote comparisons to the *pilT^{WA}* parent. (**C**) Representative images of surface piliation (top panel) and cellular aggregation (bottom panel) for the indicated strains. Scale bar for micrographs, 3 µm. Data are representative of two independent experiments. (**D**) Distance frequency histogram for the indicated residue pairs during the MD simulation of the AF3 PilT-PilU model. Distances between the side chains of the indicated residues were measured at 0.1-ns intervals over the 500-ns simulation. Percentage on graph denotes the amount of time that the indicated side chains are <3.5 Å (dotted line). Data are compiled from two independent MD simulations.

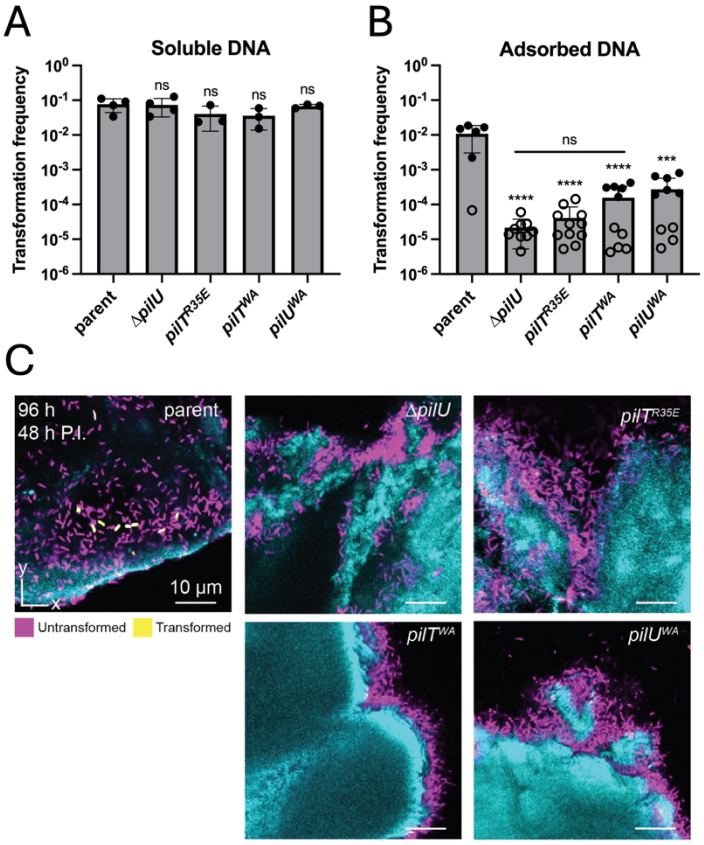

Fig. 4. **PilT-PilU$^{C\text{-}term}$ interactions are critical for motor coordination under physiologically relevant conditions.** (**A**) Chitin-dependent NT assays of the indicated *V. cholerae* strains with soluble tDNA. (**B**) Flow biofilm NT assays where tDNA was adsorbed to the chitin surface. Open circles denote replicates where no transformants were observed and the limit of detection for that sample is plotted. (**C**) Representative images of assays described in **B** highlighting transformed (yellow) and untransformed (magenta) cells within the chitin-bound biofilm. The chitin surface is shown in cyan and appears irregular in shape due to optical sectioning through the 3-dimensional shrimp shell particles used for these experiments. All data are from at least 3 independent biological replicates and shown as the mean ± SD. Statistical comparisons were made by one-way ANOVA with Tukey's multiple comparison test of the log-transformed data. ns, not significant; *** = $p < 0.001$; **** = $p < 0.0001$. Symbols directly above bars denote comparison to the parent.

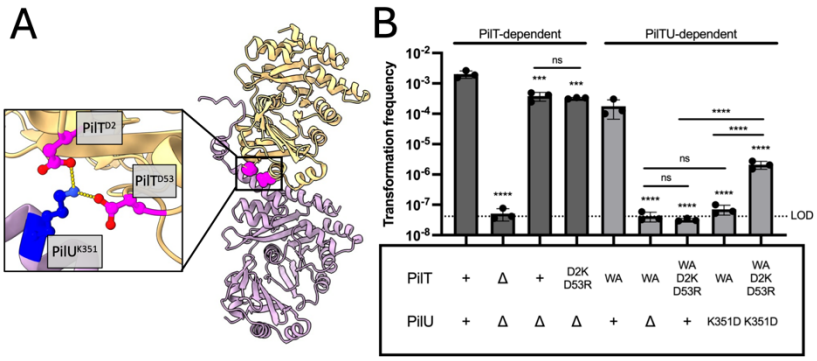

Fig. 5. **PilT-PilU$^{C\text{-}term}$ contacts are important for T4P retraction in *A. baylyi*.** (**A**) AF3 model of PilT$_{Ab}$ (orange)-PilU$_{Ab}$ (pink) interactions. Inset shows the conserved PilT$_{Ab}^{D2,D53}$-PilU$_{Ab}^{K351}$ salt bridge. (**B**) NT assays of the indicated *A. baylyi* strains. Dark gray bars denote strains that report on PilT-dependent retraction (*i.e.*, in a *pilT*$^{+}$ background where PilT ATPase activity is intact), while light grey bars denote strains that report on PilT-PilU-dependent retraction (*i.e.*, in a *pilT*^{WA} background where retraction is dependent on PilU). Data are from three independent biological replicates and shown as the mean ± SD. Statistical comparisons were made by one-way ANOVA with Tukey's multiple comparison test of the log-transformed data. ns, not significant; *** = $p < 0.001$; **** = $p < 0.0001$. Symbols above the dark grey bars denote comparisons to the parent, while symbols above the light grey bars denote comparisons to *pilT*^{WA}.

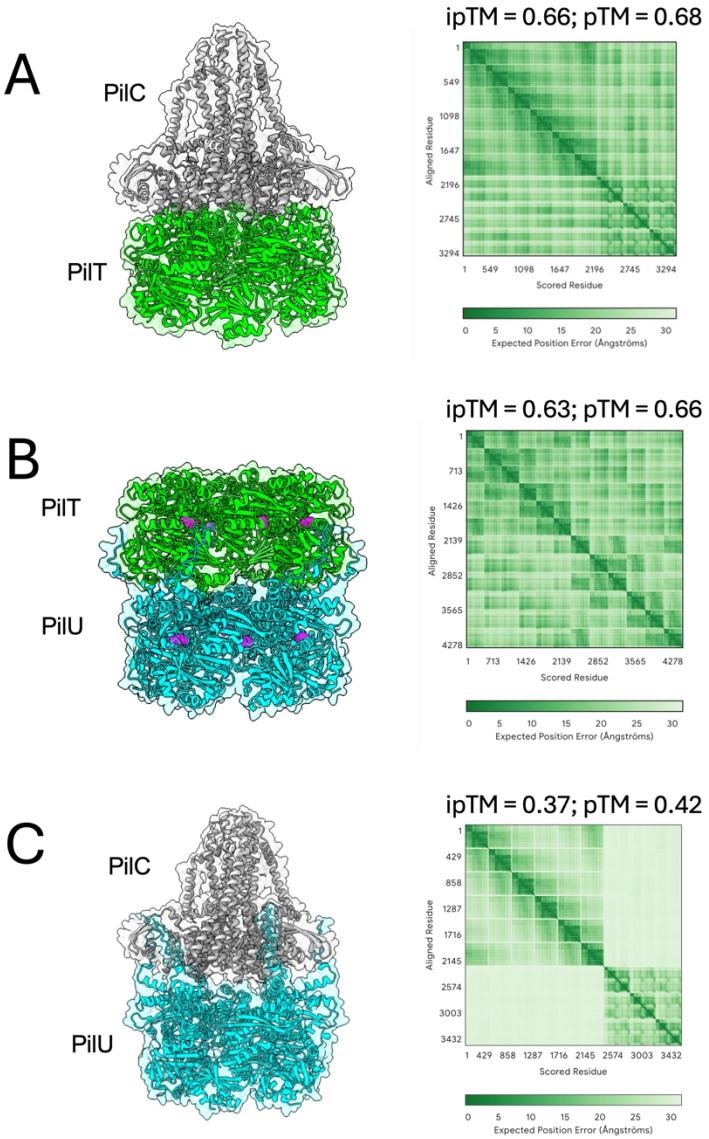

Fig. S1. **AF3 models of PilT-PilC, PilT-PilU, and PilU-PilC interactions.** AF3 models (left) of the indicated *V. cholerae* proteins with their respective PAE maps and confidence scores (right). (**A**) PilT(x6)-PilC(x3) and (**B**) PilT(x6)-PilU(x6) were used to generate the PilC-PilT-PilU hybrid complex shown in **Fig. 1A.** The magenta spheres in **B** denote the Walker A residues in PilT and PilU ($PilT^{K136A}$ and $PilU^{K134A}$, respectively). (**C**) The PilU(x6)-PilC(x3) AF3 model had very low confidence metrics, suggesting that these proteins may not directly interact.

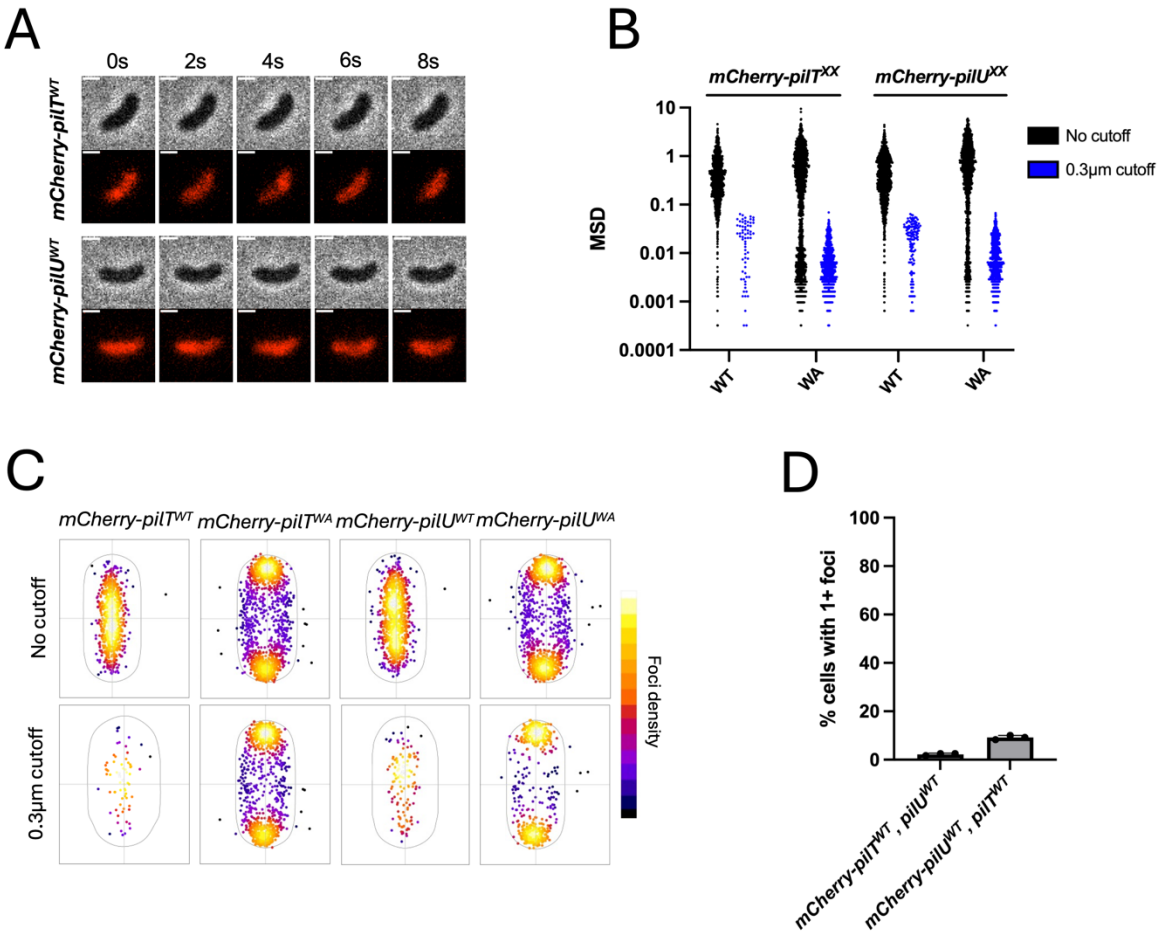

Fig. S2. *mCherry-pilT^{WA}* and *mCherry-pilU^{WA}* form foci at the cell periphery. (**A**) Representative montage of timelapse imaging for the indicated strains highlights the lack of fluorescent foci in these backgrounds. Scale bars, 1 μM. (**B**) Mean-squared displacement (MSD) values of motor foci in the indicated strains. Black scatter plots represent MSD data collected with no cutoff for the distance foci can move between frames of the 10 s timelapse. Blue scatter plots represent MSD data collected for the same strains with a 0.3 μm cutoff for foci movement between frames. (**C**) Scatter plots of the localization of fluorescent foci in the same strains from **B** with and without a 0.3 μm distance cutoff. (**D**) Motor localization assays were performed on the indicated *V. cholerae* strains. For each strain, the percentage of cells (*n* = 120 cells analyzed) with at least one fluorescent focus that moves less than 0.3 μm between frames was determined. Data are from three independent biological replicates and are shown as the mean ± SD.

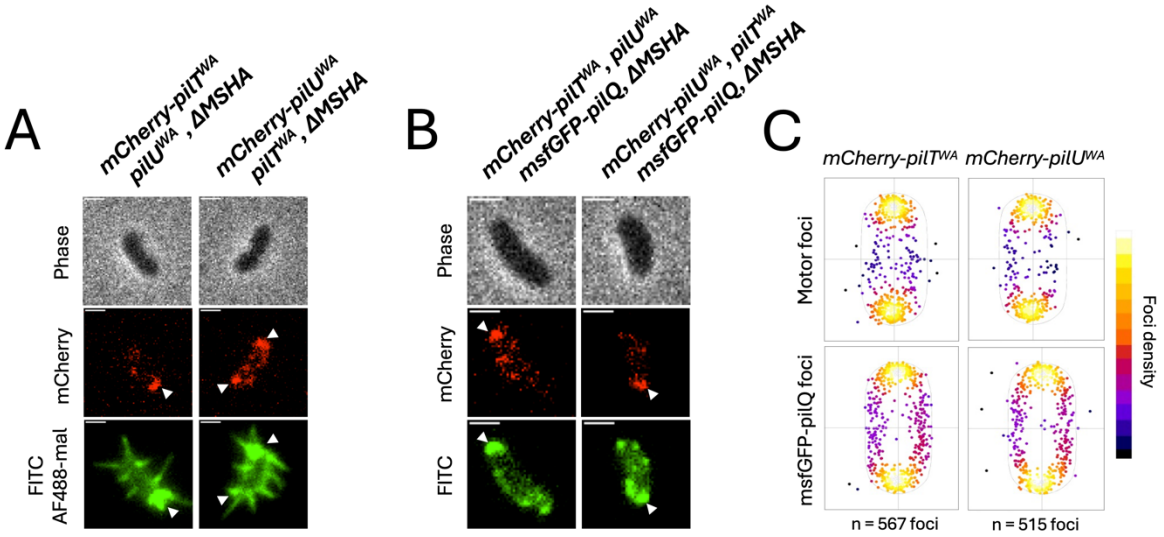

Fig. S3. PilT and PilU foci colocalize with competence T4P machines. (**A**) Δ*MSHA* cells expressing *mCherry-pilT*^{WA} or *mCherry-pilU*^{WA} as indicated were labeled with AF488-mal to colocalize motor foci and competence pili. White carats denote motor focus localization at the base of competence T4P filaments. Scale bar, 1 µm. (**B**) Δ*MSHA* cells expressing *msfGFP-pilQ* and *mCherry-pilT*^{WA} or *mCherry-pilU*^{WA} as indicated. The representative images show motor foci colocalizing with msfGFP-PilQ foci (mCherry-PilT^{WA} and mCherry-PilU^{WA} foci colocalize with msfGFP-PilQ foci at a frequency of 99.3 ± 0.7% and 98.1% ± 1%, respectively). Scale bar, 1 µm. (**C**) Scatter heat maps denote the localization of motor foci and PilQ foci from the experiments described in **B**. These heat maps highlight that both PilT/PilU motor foci and PilQ foci are biased towards the cell poles. Data in **A-C** are representative of *n* = 3 biological replicates, and colocalization frequency is reported as the mean ± SD.

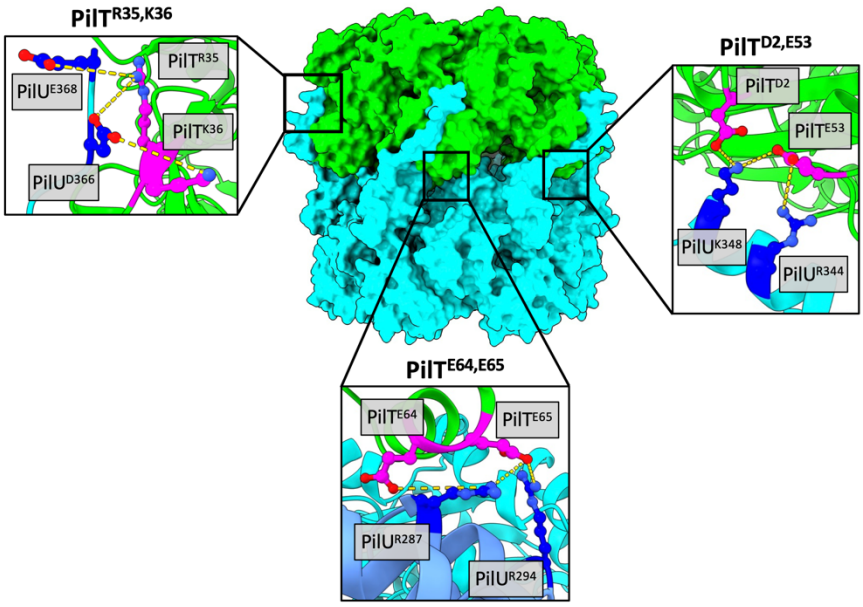

Fig. S4. Contact analysis of the AF3 PilT-PilU model reveals three putative intermolecular salt bridges. AF3 model of the PilT (green)-PilU (cyan) complex. Insets show the residues involved in the three putative intermolecular salt bridges with PilT residues colored in magenta and PilU residues colored in blue.

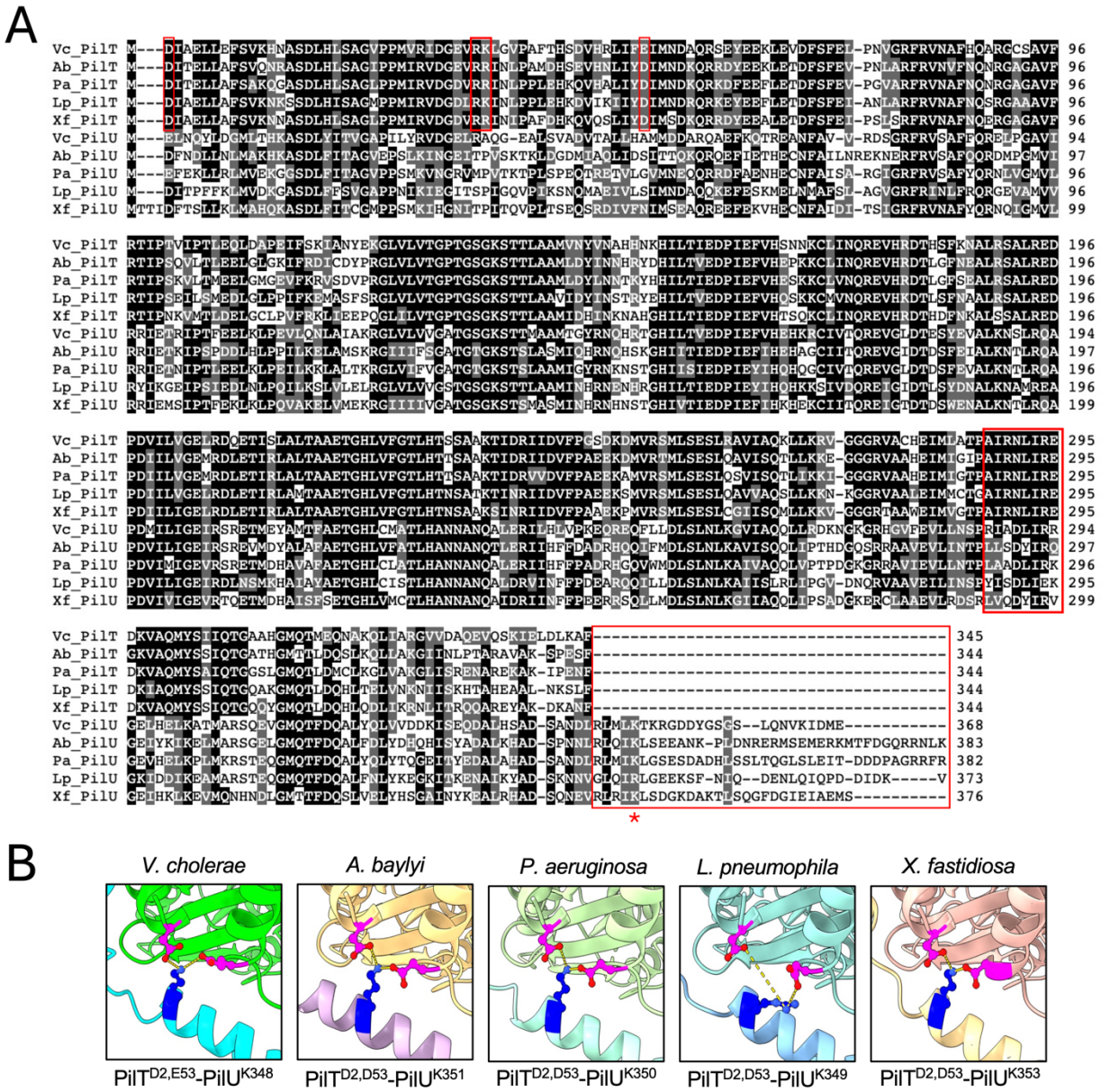

Fig. S5. Sequence and structural alignments uncover conserved elements in PilT and PilU homologs. (**A**) Multiple sequence alignment of PilT and PilU homologs from the following bacterial species: Vc = *Vibrio cholerae*, Ab = *Acinetobacter baylyi*, Pa = *Pseudomonas aeruginosa*, Lp = *Legionella pneumophila*, and Xf = *Xylella fastidiosa*. Red boxes denote conservation of the $PilT_{Vc}$ residues studied (D2, R35, K36, and E53), the PilT AIRNLIRE motif, and the extended C-terminus that is unique to PilU homologs. The red asterisk highlights conservation of the $PilU_{Vc}^{K348}$ residue among PilU homologs. (**B**) AF3 models of PilT-PilU complexes from the indicated species highlights the predicted conservation of the experimentally validated $PilT_{Vc}^{D2,E53}$-$PilU_{Vc}^{K348}$ intermolecular salt bridge.

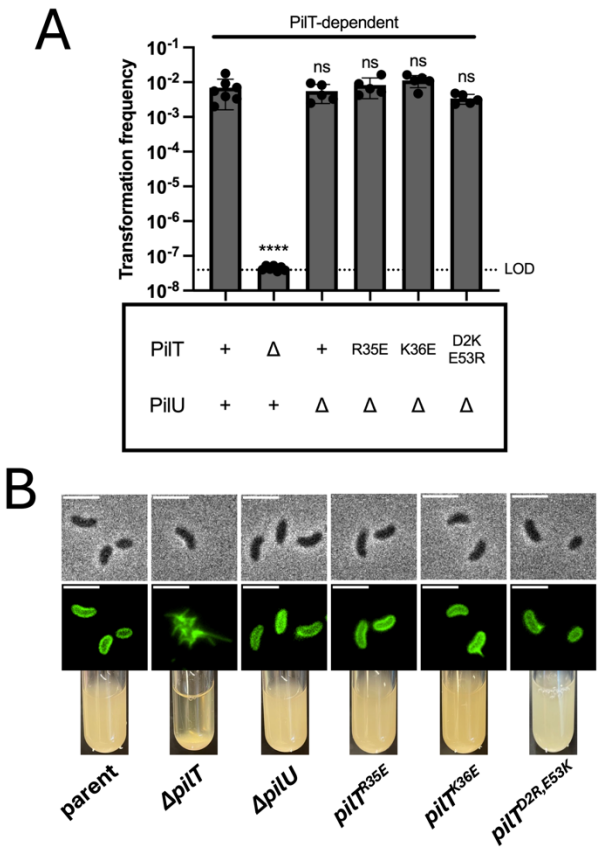

Fig. S6. Mutating the PilT residues in the putative intermolecular salt bridges does not impact PilT-dependent retraction. (**A**) NT assays of the indicated *V. cholerae* strains demonstrates that mutating the residues involved in putative PilT-PilU intermolecular salt bridges does not impact PilT-dependent retraction (*i.e.*, in a background where PilT ATPase activity is intact). Data are from five independent biological replicates and shown as the mean ± SD. (**B**) Representative images of surface piliation (top panel) and cellular aggregation (bottom panel) for the indicated strains. Scale bar for micrographs, 3 µm. Data are representative of two independent experiments. Statistical comparisons were made by one-way ANOVA with Tukey's multiple comparison test of the log-transformed data. ns, not significant; **** = $p < 0.0001$. Symbols directly above bars denote comparisons to the parent.

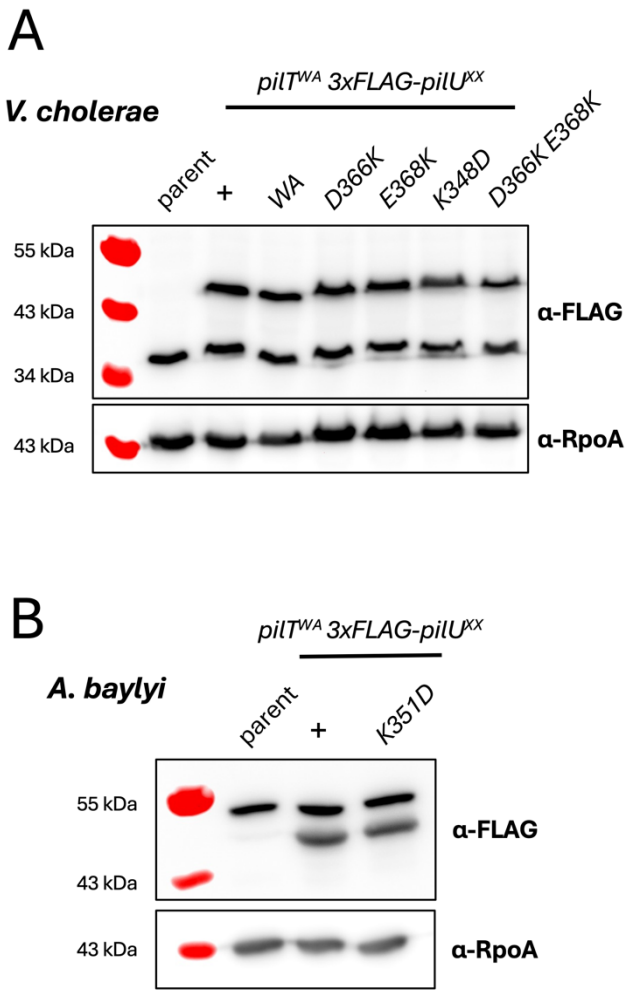

Fig. S7. PilU point mutants do not impact PilU steady-state levels. Western blot analysis to assess steady-state levels of 3xFLAG-PilU and RpoA (loading control) from whole-cell lysates of the indicated point mutants in (**A**) *V. cholerae* and (**B**) *A. baylyi*. 3xFLAG-PilU is ~45kDa in *V. cholerae* and ~47kDa in *A. baylyi*. Notably, in anti-FLAG blots there is a distinct nonspecific band in both species (demarcated by the parent strain that lacks any FLAG-tagged constructs), which serves as an additional loading control. Blots in **A** and **B** are representative of three independent biological replicates.

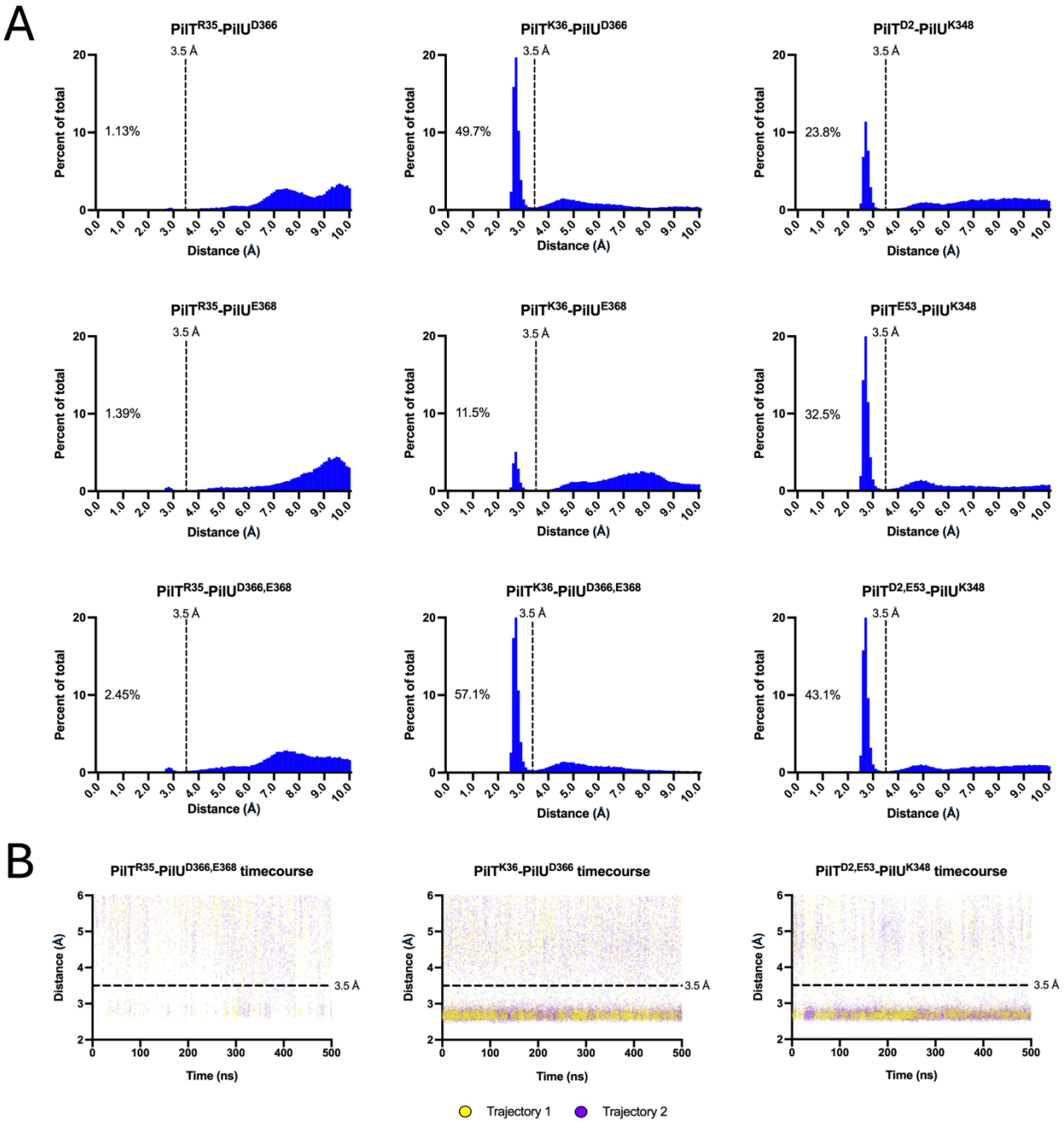

Fig. S8. MD simulations of the AF3 PilT-PilU complex predict stable salt bridges between PilT^{K36}-PilU^{D366} and PilT^{D2,E53}-PilU^{K348}. (**A**) Distance frequency histogram for the indicated residue pairs during the MD simulation of the AF3 PilT-PilU model. Distances between the side chains of the indicated residues were measured at 0.1-ns intervals over the 500-ns simulation. Percentage on graph denotes the amount of time that the indicated side chains are <3.5 Å (dotted line). Data are compiled from two independent MD simulations. (**B**) Time-course scatter plots of distance measurements for the indicated residue pairs. Trajectories 1 and 2 represent two independent replicates of the MD simulations.

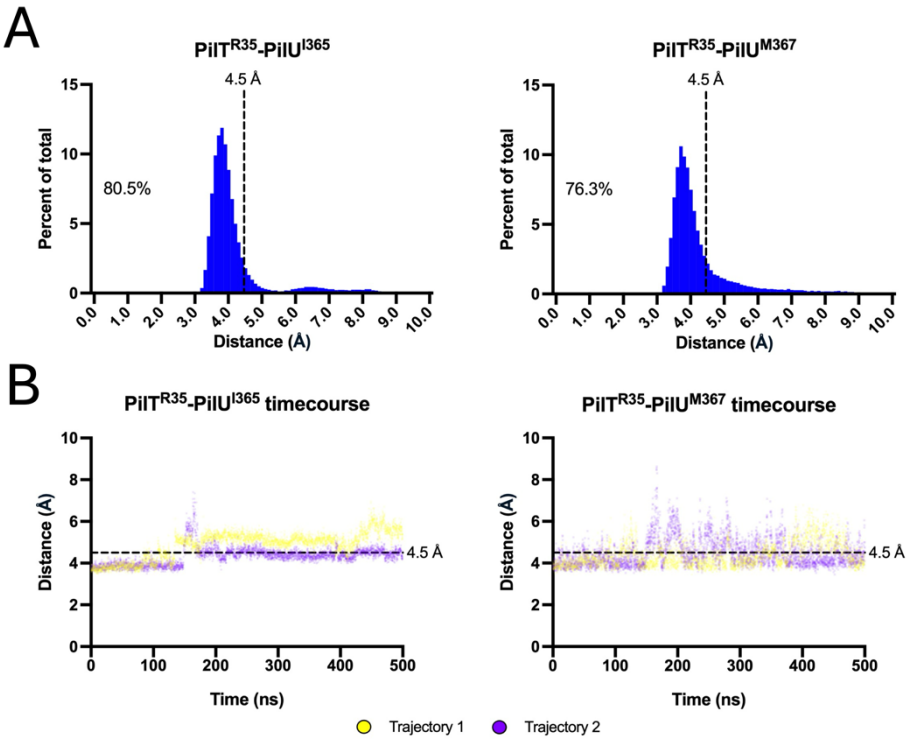

Fig. S9. AF3-MD simulations support PilT^{R35}-PilU^{I365,M367} interactions. (**A**) Distance frequency histograms of the indicated residues. Distances between the side chains of the indicated residues were recorded at 0.1-ns intervals over the 500-ns MD simulation. Percentages denote the amount of time that the residues were within 4.5 Å (dotted line). Data are compiled from two independent MD simulations. (**B**) Time-course scatter plots of the distance measurements for the indicated interactions. Trajectories 1 and 2 represent two independent replicates of the MD simulation.

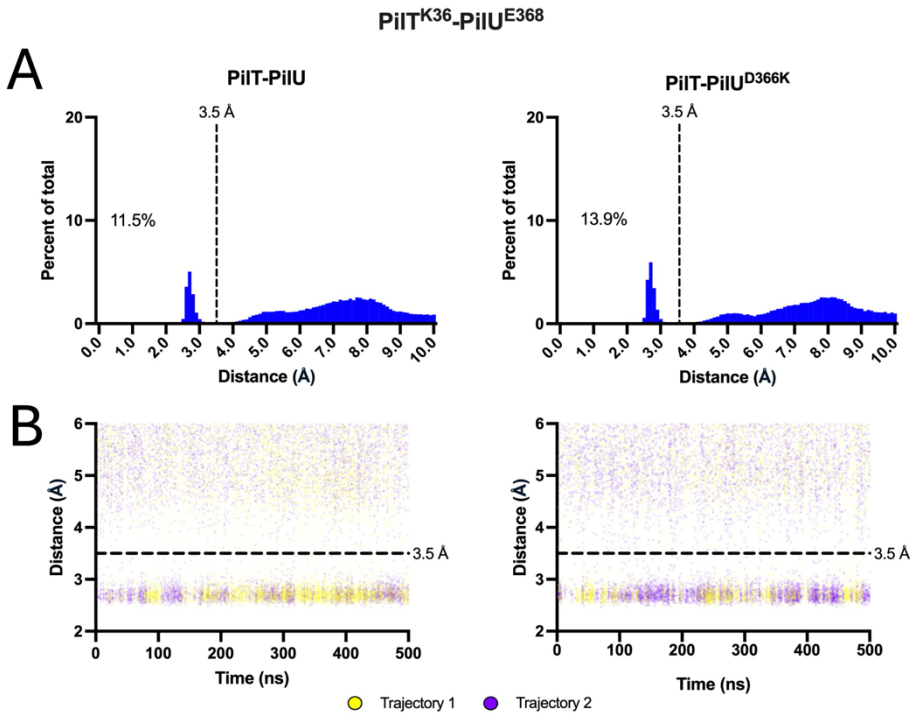

Fig. S10. MD simulations predict intermediate contact between PilT^{K36}-PilU^{E368} in the PilT-PilU and PilT-PilU^{D366K} AF3 complexes. (**A**) Distance frequency histograms of PilT^{K36}-PilU^{E368} in the PilT-PilU vs PilT-PilU^{D366K} MD simulations as indicated. Distances between the side chains were measured at 0.1-ns intervals over the 500-ns simulation. Percentages on the histograms denote the amount of time the PilT^{K36E} and PilU^{E368K} are <3.5 Å apart (dotted line). Data are compiled from two independent MD simulations. (**B**) Timecourse scatter plots of the distances between PilT^{K36E}-PilU^{E368K} in the PilT-PilU vs PilT-PilU^{E368K} MD simulations as indicated. Trajectories 1 and 2 represent two independent replicates of the MD simulation. In **A**, the data for the PilT-PilU complex is identical to the data presented in **Fig. S8** and are included here for ease of comparison.

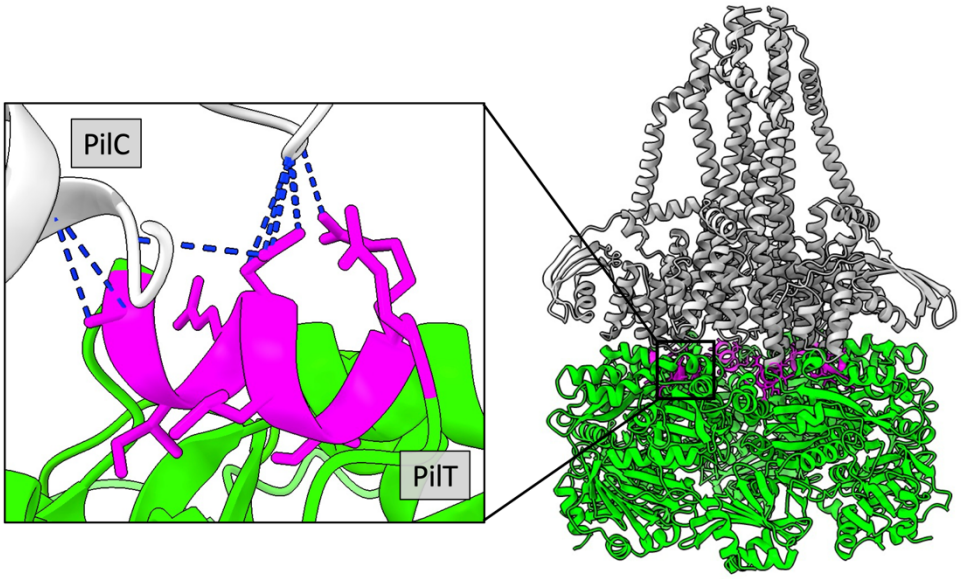

Fig. S11. AF3 predicts that the AIRNLIRE motif is at the PilC-PilT interface. AF3 model of the PilC(3x)-PilT(6x) complex. Residues of the AIRNLIRE motif (PilT$^{A288-E295}$) are colored in magenta. The inset shows a slice of the PilT-PilC model for a better view of the AIRNLIRE motif at the PilC-PilT interface. The blue dashed lines represent contacts predicted between the PilT AIRNLIRE motif and PilC.

964 **Table S1**. Strains used in this study
965

Strain #	Genotype	Figure	Use in manuscript	Name in manuscript
AET249 / SAD4023	E7946 Sm^R, P_{tac}-*tfoX*, Δ*luxO*, *pilA*^{S67C}, Δ*pilT*::Smx^R *pilU*^{K134A}, Δ*lacZ*::$Spec^R$-P_{pilT}-*mCherry*-L5-*pilT*^{K136A}	Fig 1b; Fig 1c; Fig S2	Fluorescence microscopy foci quantification	*mCherry-pilT*^{WA}, *pilU*^{WA}
AET396 / SAD4024	E7946 Sm^R, P_{tac}-*tfoX*, Δ*luxO*, *pilA*^{S67C}, Δ*pilT*::SmxR *pilU*^{K134A}, Δ*lacZ*::$Spec^R$-P_{pilT}-*mCherry*-L5-*pilT*^{K136A}, Δ*MSHA*::$Carb^R$, Δ*pilC*::Cm^R	Fig 1c	Fluorescence microscopy foci quantification	*mCherry-pilT*^{WA}, *pilU*^{WA}, Δ*platform*
AET146 / SAD4025	E7946 Sm^R, P_{tac}-*tfoX*, Δ*luxO*, *pilA*^{S67C}, Δ*lacZ*::$Spec^R$-P_{pilT}-*mCherry*-L5-*pilT*^{K136A}, Δ*pilTU*::Tm^R	Fig 1c; Fig 2e	Fluorescence microscopy foci quantification	*mCherry-pilT*^{WA}, Δ*pilU*
AET222 / SAD4026	E7946 *Sm*^{R}, P_{tac}-*tfoX*, Δ*luxO*, *pilA*^{S67C}, Δ*lacZ*::$Spec^R$-P_{pilT}-*mCherry*-L5-*pilT*^{K136A}, Δ*pilTU*::Tm^R, Δ*MSHA*::$Carb^R$, Δ*pilC*::Cm^R	Fig 1c	Fluorescence microscopy foci quantification	*mCherry-pilT*^{WA}, Δ*pilU,* Δ*platform*
AET159 / SAD4027	E7946 Sm^R, P_{tac}-*tfoX*, Δ*luxO*, *pilA*^{S67C}, Δ*pilT*::Smx^R *mCherry*-L5-*pilU*^{K134A}, Δ*lacZ*::$Spec^R$-P_{pilT}-*pilT*^{K136A}	Fig 1b; Fig 1d; Fig 2d; Fig S2	Fluorescence microscopy foci quantification	*mCherry-pilU*^{WA}, *pilT*^{WA}
AET205 / SAD4028	E7946 Sm^R, P_{tac}-*tfoX*, Δ*luxO*, *pilA*^{S67C}, Δ*pilT*::Smx^R *mCherry*-L5-*pilU*^{K134A}, Δ*lacZ*::$Spec^R$-P_{pilT}-*pilT*^{K136A}, Δ*MSHA*::$Carb^R$, Δ*pilC*::Cm^R	Fig 1d	Fluorescence microscopy foci quantification	*mCherry-pilU*^{WA}, *pilT*^{WA}, Δ*platform*
AET153 / SAD4029	E7946 Sm^R, P_{tac}-*tfoX*, Δ*luxO*, *pilA*^{S67C}, Δ*pilT*::Smx^R *mCherry*-L5-*pilU*^{K134A}	Fig 1d; Fig 2d	Fluorescence microscopy foci quantification	*mCherry-pilU*^{WA}, Δ*pilT*
AET155 / SAD4030	E7946 Sm^R, P_{tac}-*tfoX*, Δ*luxO*, *pilA*^{S67C}, Δ*pilT*::Smx^R *gfp*-L5-*pilU*^{K134A}, Δ*lacZ*::$Spec^R$-P_{pilT}-*pilT*^{K136A}-L5-*mCherry*	Fig 1e; Fig 1f	Fluorescence co-localization	*pilT*^{WA}*-mCherry, gfp-pilU*^{WA}
TND0905 / SAD2468 / (18, 26)	E7946 Sm^R, P_{tac}-*tfoX*, Δ*luxO*, *pilA*^{S67C}	Fig 2b-c; Fig S6; Fig S7a	Transformation, pilus labeling, cellular aggregation assays, and western blots	Parent
AET111 / SAD4031	E7946 Sm^R, P_{tac}-*tfoX*, Δ*luxO*, *pilA*^{S67C}, Δ*pilT*::Smx^R	Fig 2b-c; Fig S6	Transformation, pilus labeling, and cellular aggregation assays	Δ*pilT*
TND1515 / SAD4032	E7946 Sm^R, P_{tac}-*tfoX*, Δ*luxO*, *pilA*^{S67C}, Δ*pilU*::Tm^R	Fig 2b-c; Fig S6	Transformation, pilus labeling, and cellular aggregation assays	Δ*pilU*

TND4516 / SAD4033	E7946 Sm^R, P_{tac}-*tfoX*, Δ*luxO*, *pilA*^{S67C}, Δ*pilT*::Smx^R, Δ*lacZ*::$Spec^R$-PpilT-*pilT*^{K136A}	Fig 2b-c; Fig 3b-c	Transformation, pilus labeling, and cellular aggregation assays	*pilT*^{WA}
TND4360 / SAD4034	E7946 Sm^R, P_{tac}-*tfoX*, Δ*luxO*, *pilA*^{S67C}, Δ*pilTU*::Tm^R, Δ*lacZ*::$Spec^R$-P_{pilT}-*pilT*^{K136A}	Fig 2b-c; Fig 3b-c	Transformation, pilus labeling, and cellular aggregation assays	*pilT*^{WA}, Δ*pilU*
TND4361 / SAD4035	E7946 Sm^R, P_{tac}-*tfoX*, Δ*luxO*, *pilA*^{S67C}, Δ*pilTU*::Tm^R, Δ*lacZ*::$Spec^R$-P_{pilT}-*pilT*^{E64A,E65A}	Fig 2b-c	Transformation, pilus labeling, and cellular aggregation assays	*pilT*^{E64A,E65A}
TND4362 / SAD4036	E7946 Sm^R, P_{tac}-*tfoX*, Δ*luxO*, *pilA*^{S67C}, Δ*pilTU*::Tm^R, Δ*lacZ*::$Spec^R$-P_{pilT}-*pilT*^{R35A,K36A}	Fig 2b-c	Transformation, pilus labeling, and cellular aggregation assays	*pilT*^{R35A,K36A}
AET265 / SAD4037	E7946 Sm^R, P_{tac}-*tfoX*, Δ*luxO*, *pilA*^{S67C}, Δ*pilTU*::Tm^R, Δ*lacZ*::$Spec^R$-P_{pilT}-*pilT*^{D2A,E53A}	Fig 2b-c	Transformation, pilus labeling, and cellular aggregation assays	*pilT*^{D2A,E53A}
AET112 / SAD4038	E7946 Sm^R, P_{tac}-*tfoX*, Δ*luxO*, *pilA*^{S67C}, Δ*pilT*::Smx^R, Δ*lacZ*::$Spec^R$-P_{pilT}-*pilT*^{E64A,E65A,K136A}	Fig 2b-c	Transformation, pilus labeling, and cellular aggregation assays	*pilT*^{WA,E64A,E65A}
AET113 / SAD4039	E7946 Sm^R, P_{tac}-*tfoX*, Δ*luxO*, *pilA*^{S67C}, Δ*pilT*::Smx^R, Δ*lacZ*::$Spec^R$-P_{pilT}-*pilT*^{R35A,K36A,K136A}	Fig 2b-c	Transformation, pilus labeling, and cellular aggregation assays	*pilT*^{WA,R35A,K36A}
AET275 / SAD4040	E7946 Sm^R, P_{tac}-*tfoX*, Δ*luxO*, *pilA*^{S67C}, Δ*pilT*::Smx^R, Δ*lacZ*::$Spec^R$-P_{pilT}-*pilT*^{D2A,E53A,K136A}	Fig 2b-c	Transformation, pilus labeling, and cellular aggregation assays	*pilT*^{WA,D2A,E53A}
AET262 / SAD4041	E7946 Sm^R, P_{tac}-*tfoX*, Δ*luxO*, *pilA*^{S67C}, Δ*pilT*::Smx^R *mCherry*-L5-*pilU*^{K134A}, Δ*lacZ*::$Spec^R$-P_{pilT}-*pilT*^{E64A,E65A,K136A}	Fig 2d	Fluorescence microscopy foci quantification	*mCherry-pilU*^{WA}, *pilT*^{WA,E64A,E65A}
AET263 / SAD4042	E7946 Sm^R, P_{tac}-*tfoX*, Δ*luxO*, *pilA*^{S67C}, Δ*pilT*::Smx^R *mCherry*-L5-*pilU*^{K134A}, Δ*lacZ*::$Spec^R$-P_{pilT}-*pilT*^{R35A,K36A,K136A}	Fig 2d	Fluorescence microscopy foci quantification	*mCherry-pilU*^{WA}, *pilT*^{WA,R35A,K36A}
AET277 / SAD4043	E7946 Sm^R, P_{tac}-*tfoX*, Δ*luxO*, *pilA*^{S67C}, Δ*pilT*::Smx^R *mCherry*-L5-*pilU*^{K134A}, Δ*lacZ*::$Spec^R$-P_{pilT}-*pilT*^{D2A,E53A,K136A}	Fig 2d	Fluorescence microscopy foci quantification	*mCherry-pilU*^{WA}, *pilT*^{WA,D2A,E53A}
AET271 / SAD4044	E7946 Sm^R, P_{tac}-*tfoX*, Δ*luxO*, *pilA*^{S67C}, Δ*pilTU*::Tm^R, Δ*lacZ*::$Spec^R$-P_{pilT}-*mCherry*-L5-*pilT*^{E64A,E65A,K136A}	Fig 2e	Fluorescence microscopy foci quantification	*mCherry-pilT*$^{WA,E64A\ E65A}$

AET270 / SAD4045	E7946 Sm^R, P_{tac}-*tfoX*, Δ*luxO*, *pilA*^{S67C}, Δ*pilTU*::Tm^R, Δ*lacZ*::$Spec^R$-P_{pilT}-*mCherry*-L5-*pilT*^{R35A,K36A,K136A}	Fig 2e	Fluorescence microscopy foci quantification	*mCherry-pilT*$^{WA,R35A\ K36A}$
AET278 / SAD4046	E7946 Sm^R, P_{tac}-*tfoX*, Δ*luxO*, *pilA*^{S67C}, Δ*pilTU*::Tm^R, Δ*lacZ*::$Spec^R$-P_{pilT}-*mCherry*-L5-*pilT*^{D2A,E53A,K136A}	Fig 2e	Fluorescence microscopy foci quantification	*mCherry-pilT*^{WA,D2A,E53A}
AET189 / SAD4047	E7946 Sm^R, P_{tac}-*tfoX*, Δ*luxO*, *pilA*^{S67C}, Δ*pilT*::Smx^R, Δ*lacZ*::$Spec^R$-P_{pilT}-*pilT*^{R35E,K136A}	Fig 3b-c	Transformation, pilus labeling, and cellular aggregation assays	*pilT*^{WA,R35E}
TND4578 / SAD4048	E7946 Sm^R, P_{tac}-*tfoX*, Δ*luxO*, *pilA*^{S67C}, Δ*pilT*::Smx^R *pilU*^{D366K,E368K}, Δ*lacZ*::$Spec^R$-P_{pilT}-*pilT*^{K136A}	Fig 3b-c	Transformation, pilus labeling, and cellular aggregation assays	*pilT*^{WA}, *pilU*^{D366K,E368K}
AET391 / SAD4049	E7946 Sm^R, P_{tac}-*tfoX*, Δ*luxO*, *pilA*^{S67C}, Δ*pilT*::Smx^R *pilU*^{D366K,E368K}, Δ*lacZ*::$Spec^R$-P_{pilT}-*pilT*^{R35E,K136A}	Fig 3b-c	Transformation, pilus labeling, and cellular aggregation assays	*pilT*^{WA,R35E}, *pilU*^{D366K,E368K}
AET190 / SAD4050	E7946 Sm^R, P_{tac}-*tfoX*, Δ*luxO*, *pilA*^{S67C}, Δ*pilT*::Smx^R, Δ*lacZ*::$Spec^R$-P_{pilT}-*pilT*^{K36E,K136A}	Fig 3b-c	Transformation, pilus labeling, and cellular aggregation assays	*pilT*^{WA,K36E}
AET200 / SAD4051	E7946 Sm^R, P_{tac}-*tfoX*, Δ*luxO*, *pilA*^{S67C}, Δ*pilT*::Smx^R *pilU*^{D366K}, Δ*lacZ*::$Spec^R$-P_{pilT}-*pilT*^{K136A}	Fig 3b-c	Transformation, pilus labeling, and cellular aggregation assays	*pilT*^{WA}, *pilU*^{D366K}
AET201 / SAD4052	E7946 Sm^R, P_{tac}-*tfoX*, Δ*luxO*, *pilA*^{S67C}, Δ*pilT*::Smx^R *pilU*^{E368K}, Δ*lacZ*::$Spec^R$-P_{pilT}-*pilT*^{K136A}	Fig 3b-c	Transformation, pilus labeling, and cellular aggregation assays	*pilT*^{WA}, *pilU*^{E368K}
AET198 / SAD4053	E7946 Sm^R, P_{tac}-*tfoX*, Δ*luxO*, *pilA*^{S67C}, Δ*pilT*::Smx^R *pilU*^{D366K}, Δ*lacZ*::$Spec^R$-P_{pilT}-*pilT*^{K36E,K136A}	Fig 3b-c	Transformation, pilus labeling, and cellular aggregation assays	*pilT*^{WA,K36E}, *pilU*^{D366K}
AET199 / SAD4054	E7946 Sm^R, P_{tac}-*tfoX*, Δ*luxO*, *pilA*^{S67C}, Δ*pilT*::Smx^R *pilU*^{E368K}, Δ*lacZ*::$Spec^R$-P_{pilT}-*pilT*^{K36E,K136A}	Fig 3b-c	Transformation, pilus labeling, and cellular aggregation assays	*pilT*^{WA,K36E}, *pilU*^{E368K}
AET475 / SAD4106	E7946 Sm^R, P_{tac}-*tfoX*, Δ*luxO*, *pilA*^{S67C}, Δ*pilT*::Smx^R *pilU*^{D366K,E368K}, Δ*lacZ*::$Spec^R$-P_{pilT}-*pilT*^{K36E,K136A}	Fig 3b-c	Transformation, pilus labeling, and cellular aggregation assays	*pilT*^{WA,K36E}, *pilU*^{D366K,E368K}
AET345 / SAD4055	E7946 Sm^R, P_{tac}-*tfoX*, Δ*luxO*, *pilA*^{S67C}, Δ*pilT*::Smx^R, Δ*lacZ*::$Spec^R$-P_{pilT}-*pilT*^{D2K,E53R,K136A}	Fig 3b-c	Transformation, pilus labeling, and cellular aggregation assays	*pilT*^{WA,D2K,E53R}

AET337 / SAD4056	E7946 Sm^R, P_{tac}-*tfoX*, Δ*luxO*, *pilA*^{S67C}, Δ*pilT*::Smx^R *pilU*^{K348D}, Δ*lacZ*::$Spec^R$-P_{pilT}-*pilT*^{K136A}	Fig 3b-c	Transformation, pilus labeling, and cellular aggregation assays	*pilT*^{WA}, *pilU*^{K348D}
AET358 / SAD4057	E7946 Sm^R, P_{tac}-*tfoX*, Δ*luxO*, *pilA*^{S67C}, Δ*pilT*::Smx^R *pilU*^{K348D}, Δ*lacZ*::$Spec^R$-P_{pilT}-*pilT*^{D2K,E53R,K136A}	Fig 3b-c	Transformation, pilus labeling, and cellular aggregation assays	*pilT*^{WA,D2K,E53R}, *pilU*^{K348D}
TND3433 / SAD4058 / (24)	Δ*VC1807*::Cm^R-P_{tac}-*gfp*::*parST1*, Δ*lacZ*::$Spec^R$-P_{tac}-*mKate2*	Fig 4a-c	Chitin biofilm natural transformation assays	Parent (chitin biofilm NT assays)
TND4366 / SAD4059 / (24)	Δ*VC1807*::Cm^R-P_{tac}-*gfp*::*parST1*, Δ*lacZ*::$Spec^R$-P_{tac}-*mKate2*, Δ*pilU*::Tm^R	Fig 4a-c	Chitin biofilm natural transformation assays	Δ*pilU* (chitin biofilm NT assays)
AET254 / SAD4060	Δ*VC1807*::Cm^R-P_{tac}-*gfp*::*parST1*, Δ*lacZ*::$Spec^R$-P_{tac}-*mKate2*, *pilT*^{R35E}	Fig 4a-c	Chitin biofilm natural transformation assays	*pilT*^{R35E} (chitin biofilm NT assays)
AET401 / SAD4107	Δ*VC1807*::Cm^R-P_{tac}-*gfp*::*parST1*, Δ*lacZ*::$Spec^R$-P_{tac}-*mKate2*, *pilT*^{K136A}	Fig 4a-c	Chitin biofilm natural transformation assays	*pilT*^{K136A} (chitin biofilm NT assays)
AET402 / SAD4108	Δ*VC1807*::Cm^R-P_{tac}-*gfp*::*parST1*, Δ*lacZ*::$Spec^R$-P_{tac}-*mKate2*, *pilU*^{K134A}	Fig 4a-c	Chitin biofilm natural transformation assays	*pilU*^{K134A} (chitin biofilm NT assays)
TND0428 / SAD2537 / (18)	*comP*^{T129C}	Fig 5b; Fig S7b	*A. baylyi* natural transformation assays and Western blots	Parent (*A. baylyi* NT assays and Westerns)
TND0799 / SAD2544 / (18)	*comP*^{T129C}, Δ*pilTU*::Zeo^R	Fig 5b	*A. baylyi* natural transformation assays	Δ*pilT* (*A. baylyi* NT assays)
TND0798 / SAD2543 / (18)	*comP*^{T129C}, Δ*pilU*::Zeo^R	Fig 5b	*A. baylyi* natural transformation assays	Δ*pilU* (*A. baylyi* NT assays)
AET392 / SAD4061	*comP*^{T129C}, *pilT*^{D2K,D53R} Δ*pilU*::Zeo^R	Fig 5b	*A. baylyi* natural transformation assays	*pilT*^{D2K,D53R} (*A. baylyi* NT assays)
TND1122 / SAD2540 / (18)	*comP*^{T129C}, *pilT*^{K136A}	Fig 5b	*A. baylyi* natural transformation assays	*pilT*^{WA} (*A. baylyi* NT assays)

TND1135 / SAD2538 / (18)	*comP*^{T129C}, *pilT*^{K136A} Δ*pilU*::Zeo^{R}	Fig 5b	*A. baylyi* natural transformation assays	*pilT*^{WA}, Δ*pilU* (*A. baylyi* NT assays)
AET316 / SAD4062	*comP*^{T129C}, *pilT*^{D2K,D53R,K136A}	Fig 5b	*A. baylyi* natural transformation assays	*pilT*^{WA,D2K,D53R} (*A. baylyi* NT assays)
AET302 / SAD4063	*comP*^{T129C}, *pilT*^{K136A} *pilU*^{K351D}	Fig 5b	*A. baylyi* natural transformation assays	*pilT*^{WA}, *pilU*^{K351D} (*A. baylyi* NT assays)
AET373 / SAD4064	*comP*^{T129C}, *pilT*^{D2K,D53R,K136A} *pilU*^{K351D}	Fig 5b	*A. baylyi* natural transformation assays	*pilT*^{WA,D2K,D53R}, *pilU*^{K351D} (*A. baylyi* NT assays)
AET369 / SAD4065	E7946 Sm^{R}, P$_{tac}$-*tfoX*, Δ*luxO*, *pilA*^{S67C}, Δ*pilT*::Smx^{R}, Δ*lacZ*::Spec^{R}-P$_{pilT}$-*mCherry*-L5-*pilT*	Fig S2	Fluorescence microscopy foci quantification	*mCherry-pilT*$^{+}$, *pilU*$^{+}$
AET367 / SAD4066	E7946 Sm^{R}, P$_{tac}$-*tfoX*, Δ*luxO*, *pilA*^{S67C}, Δ*pilT*::Smx^{R} *mCherry*-L5-*pilU*, Δ*lacZ*::Spec^{R}-P$_{pilT}$-*pilT*	Fig S2;	Fluorescence microscopy foci quantification	*mCherry-pilU*$^{+}$, *pilT*$^{+}$
AET395 / SAD4109	E7946 Sm^{R}, P$_{tac}$-*tfoX*, Δ*luxO*, *pilA*^{S67C}, Δ*pilT*::SmxR *pilU*^{K134A}, Δ*lacZ*::Spec^{R}-P$_{pilT}$-*mCherry*-L5-*pilT*^{K136A}, Δ*MSHA*::Carb^{R}	Fig S3a	Fluorescence motor and competence pilus colocalization	*mCherry-pilT*^{WA}, *pilU*^{WA}, Δ*MSHA*
AET185 / SAD4110	E7946 Sm^{R}, P$_{tac}$-*tfoX*, Δ*luxO*, *pilA*^{S67C}, Δ*pilT*::Smx^{R} *mCherry*-L5-*pilU*^{K134A}, Δ*lacZ*::Spec^{R}-P$_{pilT}$-*pilT*^{K136A}, Δ*MSHA*::Carb^{R}	Fig S3a	Fluorescence motor and competence pilus colocalization	*mCherry-pilU*^{WA}, *pilT*^{WA}, Δ*MSHA*
AET484 / SAD4111	E7946 Sm^{R}, P$_{tac}$-*tfoX*, Δ*luxO*, *pilA*^{S67C}, Δ*pilT*::SmxR *pilU*^{K134A}, Δ*lacZ*::Spec^{R}-P$_{pilT}$-*mCherry*-L5-*pilT*^{K136A}, Δ*MSHA*::Carb^{R}, *msfGFP-pilQ*	Fig S3b-c	Fluorescence motor and PilQ colocalization quantification	*mCherry-pilT*^{WA}, *pilU*^{WA}, *msfGFP-pilQ*, Δ*MSHA*
AET483 / SAD4112	E7946 Sm^{R}, P$_{tac}$-*tfoX*, Δ*luxO*, *pilA*^{S67C}, Δ*pilT*::Smx^{R} *mCherry*-L5-*pilU*^{K134A}, Δ*lacZ*::Spec^{R}-P$_{pilT}$-*pilT*^{K136A}, Δ*MSHA*::Carb^{R}, *msfGFP-pilQ*	Fig S3b-c	Fluorescence motor and PilQ colocalization quantification	*mCherry-pilU*^{WA}, *pilT*^{WA}, *msfGFP-pilQ*, Δ*MSHA*
AET208 / SAD4067	E7946 Sm^{R}, P$_{tac}$-*tfoX*, Δ*luxO*, *pilA*^{S67C}, Δ*pilTU*::Tm^{R}, Δ*lacZ*::Spec^{R}-P$_{pilT}$-*pilT*^{R35E}	Fig S6a-b	Transformation, pilus labeling, and cellular aggregation assays	*pilT*^{R35E}
AET209 / SAD4068	E7946 Sm^{R}, P$_{tac}$-*tfoX*, Δ*luxO*, *pilA*^{S67C}, Δ*pilTU*::Tm^{R}, Δ*lacZ*::Spec^{R}-P$_{pilT}$-*pilT*^{K36E}	Fig S6a-b	Transformation, pilus labeling, and cellular aggregation assays	*pilT*^{K36E}

AET397 / SAD4069	E7946 Sm^R, P_{tac}-*tfoX*, Δ*luxO*, *pilA*^{S67C}, Δ*pilTU*::Tm^R, Δ*lacZ*::$Spec^R$-P_{pilT}-*pilT*^{D2K,E53R}	Fig S6a-b	Transformation, pilus labeling, and cellular aggregation assays	*pilT*^{D2K,E53R}
AET408 / SAD4113	E7946 Sm^R, P_{tac}-*tfoX*, Δ*luxO*, *pilA*^{S67C}, Δ*pilT*::Smx^R *3xFLAG*-L5-*pilU*, Δ*lacZ*::$Spec^R$-P_{pilT}-*pilT*^{K136A}	Fig S7a	Western blots	*pilT*^{WA}*3xFLAG-pilU*$^{+}$
AET466 / SAD4114	E7946 Sm^R, P_{tac}-*tfoX*, Δ*luxO*, *pilA*^{S67C}, Δ*pilT*::Smx^R *3xFLAG*-L5-*pilU*^{K134A}, Δ*lacZ*::$Spec^R$-P_{pilT}-*pilT*^{K136A}	Fig S7a	Western blots	*pilT*^{WA}*3xFLAG-pilU*^{K134A}
AET468 / SAD4115	E7946 Sm^R, P_{tac}-*tfoX*, Δ*luxO*, *pilA*^{S67C}, Δ*pilT*::Smx^R *3xFLAG*-L5-*pilU*^{D366K}, Δ*lacZ*::$Spec^R$-P_{pilT}-*pilT*^{K136A}	Fig S7a	Western blots	*pilT*^{WA}*3xFLAG-pilU*^{D366K}
AET477 / SAD4116	E7946 Sm^R, P_{tac}-*tfoX*, Δ*luxO*, *pilA*^{S67C}, Δ*pilT*::Smx^R *3xFLAG*-L5-*pilU*^{E368K}, Δ*lacZ*::$Spec^R$-P_{pilT}-*pilT*^{K136A}	Fig S7a	Western blots	*pilT*^{WA}*3xFLAG-pilU*^{E368K}
AET480 / SAD4117	E7946 Sm^R, P_{tac}-*tfoX*, Δ*luxO*, *pilA*^{S67C}, Δ*pilT*::Smx^R *3xFLAG*-L5-*pilU*^{K348D}, Δ*lacZ*::$Spec^R$-P_{pilT}-*pilT*^{K136A}	Fig S7a	Western blots	*pilT*^{WA}*3xFLAG-pilU*^{K348D}
AET481 / SAD4118	E7946 Sm^R, P_{tac}-*tfoX*, Δ*luxO*, *pilA*^{S67C}, Δ*pilT*::Smx^R *3xFLAG*-L5-*pilU*^{D366K,E368K}, Δ*lacZ*::$Spec^R$-P_{pilT}-*pilT*^{K136A}	Fig S7a	Western blots	*pilT*^{WA}*3xFLAG-pilU*^{D366K,E368K}
AET487 / SAD4119	*comP*^{T129C}, *pilT*^{K136A} *3xFLAG-pilU*	Fig S7b	Western blots	*pilT*^{WA}*3xFLAG-pilU*$^{+}$ (*A. baylyi*)
AET492 / SAD4120	*comP*^{T129C}, *pilT*^{K136A} *3xFLAG-pilU*^{K351D}	Fig S7b	Western blots	*pilT*^{WA}*3xFLAG-pilU*^{K351D} (*A. baylyi*)

968 **Table S2**. Primers used in this study.

SOE deletions		
Primer name	**Sequence (5' to 3')**	**Description**
ABD123	ATTCCGGGGATCCGTCGAC	Antibiotic resistance cassette F
ABD124	TGTAGGCTGGAGCTGCTTC	Antibiotic resistance cassette R
BBC374	TGGCAAAAAGCGAGAGAAGAAG	*ΔluxO* F1
BBC375	gtcgacggatccccggaatCATGAGGACATATTTTGTTTTCTGC	*ΔluxO* R1
BBC376	gaagcagctccagcctacaTAAGCGATGAGAGAATGGATCAAC	*ΔluxO* F2
BBC377	TCACACCCGAATTTCCATCATGC	*ΔluxO* R2
DOG0400	ACTTCTGGCTGAAGGTCAATTTTC	*ΔpilT/U* F1
DOG0401	gtcgacggatccccggaatCATTTAAATTCCTTAATAAAGTCTGGC	*ΔpilT* R1
DOG0402	gaagcagctccagcctacaTAGGTAGGTAAAGACAGATGGAG	*ΔpilT* F2
DOG0403	TCACGTGTTCGGCCAAAATC	*ΔpilT/U* R2
DOG0405	gtcgacggatccccggaatCATCTGTCTTTACCTACCTAAAATGC	*ΔpilU* R1
DOG0406	gaagcagctccagcctacaTAGCGATGGTTACTTTGTGCG	*ΔpilU* F2
DOG0436	AAGCGTTCTGGTTCAATCACC	*ΔMSHA* locus (*ΔVC0399-VC0414*) F1
DOG0434	gtcgacggatccccggaatCATTCTCTACCACTGCTATTTGGTTC	*ΔMSHA* locus (*ΔVC0399-VC0414*) R1
BBC2129	gaagcagctccagcctacaTAATGATTAAGCACTCAATGGATCCAG	*ΔMSHA* locus (*ΔVC0399-VC0414*) F2
BBC2130	TTTTGCATCAGCAAAATCACGC	*ΔMSHA* locus (*ΔVC0399-VC0414*) R2
DOG0575	TATGTGCAAGAGCTCAAAGGC	*ΔpilC* F1
DOG0574	gtcgacggatccccggaatCATGTTGAGGCTCGTGCTG	*ΔpilC* R1
DOG0576	gaagcagctccagcctacaTAGTATGGCGACAAACGGC	*ΔpilC* F2
DOG0577	AACCGCAGTGGTAAAGCTTTG	*ΔpilC* R2
BBC1881	TTTAAAGGGGATCAGTGACCG	*ΔVC1807*::Ab^R F1
ABD340	gtcgacggatccccggaatACGTTTCATTAGTCACCTCTATTGTTAACTTGTTC	*ΔVC1807*::Ab^R R1
ABD341	gaagcagctccagcctacaTAGTCGAAAATAAAAAAAAGAGGCTCGCCTC	*ΔVC1807*::Ab^R F2
BBC1882	CAATTTTGCTTTTGGACCATCCC	*ΔVC1807*::Ab^R R2
ABD725	GAAGCAGCTCCAGCCTACA	Detect F for all deletions (unless another F primer is provided)
BBC1661	GGCTGATTTCTTTCAAATATACCAG	*ΔluxO* detect R

DOG0407	TCATCAAGATAAGCATGAGTCAG	*ΔpilU* detect R
BBC2131	GAAATGAGAAAAGGAAAATTGCAC	*ΔMSHA* detect R
DOG0578	AATCACTAAGCTCATGAGGGC	*ΔpilC* detect R
BBC3918	ggaaaaagacccagtgcgtTCCATGTTGTCGGAATCGC	*ΔpilT* detect F (band if PilT present)
DOG0404	TTCTGCTTGCCTTGCGTC	*ΔpilT* detect R (band if PilT present)
BBC695	gaagcagctccagcctacaGAACAGGTTTAATCATGAATGACG	*ΔpilT* detect constant band F
BBC702	GTGATTGAGTATGGGCTTATGG	*ΔpilT* detect constant band R
BBC1934	GTTACAAAGTCAGGGACGTAAAG	*ΔpilT/U* (A. baylyi) F1
BBC1939	GGTATTCAGATTGATCGTCAGTTAG	*ΔpilT/U* (A. baylyi) R2
BBC1935	gtcgacggatccccggaatATCCATATTTTCCCCGAAGATCG	*ΔpilT* (A. baylyi) R1
BBC1936	gaagcagctccagcctacaTAAGAATAACGCTACTCGATCTG	*ΔpilT* (A. baylyi) F2
BBC1937	gtcgacggatccccggaatCATCGTATTGTTTTCCTCTCAGATC	*ΔpilU* (A. baylyi) R1
BBC1938	gaagcagctccagcctacaCGCCGTAATCTCAAATAAAAGAG	*ΔpilU* (A. baylyi) F2
Fluorescent fusions		
Primer name	**Sequence (5' to 3')**	**Description**
BBC1835	GCaGGTGGAAGTGGTGGAgtgagcaagggcgaggagg	*mCherry*-L5 F
BBC5106	gccagctttcgcggcagcttcgccaccagaaccgctCTTGTACAGCTCGTCCATGCCGCCGGTGGAGTG	*mCherry*-L5 R
BBC3669	ttctggtggcgaagctgccgcgaaagctggcGTGagcaagggcgaggaggataacatgg	L5-*mCherry* F
BBC3223	tccacctgctccacctgccttgtacagctcgtccatgccgccggtggag	L5-*mCherry* R
BBC279	GCaGGTGGAAGTGGTGGACGTAAAGGAGAAGAACTTTTC	*gfp*-L5 F
BBC5105	gccagctttcgcggcagcttcgccaccagaaccgctGTTGTATAGTTCATCCATGCCATG	*gfp*-L5 R
ABD332	GGCTGAACGTGGTTGTCGAAAATGAC	*ΔlacZ*::X-L5-*pilT* F1
ATP0002	tccaccacttccacctgcCATTTAAATTCCTTAATAAAGTCTGGC	X-L5-*pilT* R1
ATP0005	agcggttctggtggcgaagctgccgcgaaagctggcGATATCGCTGAGTTACTGGAAT	X-L5-*pilT* F2
ABD256	CCCAAATACGGCAACTTGGCG	*ΔlacZ*::X-L5-*pilT* R2
BBC4710	AAGACCCAGAACAACAAGCC	X-L5-*pilU* F1
JCP028	tccaccacttccacctgcCATCTGTCTTTACCTACCTAAAATGC	X-L5-*pilU* R1
ATP0015	agcggttctggtggcgaagctgccgcgaaagctggcGAGTTGAATCAATATCTGGATGGC	X-L5-*pilU* F2
DOG0403	TCACGTGTTCGGCCAAAATC	X-L5-*pilU*
ABD332	GGCTGAACGTGGTTGTCGAAAATGAC	*ΔlacZ*::*pilT*-L5-X F1

ATP0006	gccagctttcgcggcagcttcgccaccagaaccgctAAATGCTTTTAAATCCAACTCGAT	*pilT*-L5-X R1
ATP0007	gcaggtggagcaggtggaTAGGTAGGTAAAGACAGATGGAGTTGA	*pilT*-L5-X F2
ABD256	CCCAAATACGGCAACTTGGCG	*ΔlacZ*::*pilT*-L5-X R2
ATP0083	agcggttctggtggcgaagctgccgcgaaagctggcGccATCGCTGAGTTACTGGAAT	X-L5-*pilT* D2A F2
BBC1839	gcatggacgagctgtacaag	*mCherry* detect F
BBC4021	caggatgtcccaggcgaa	*mCherry* detect R
BBC1903	tcgaaagatcccaacgaaaag	*gfp* detect F
BBC3897	CAAGCGATGTACATCAGAATGGG	X-*pilT* detect R
DOG0404	TTCTGCTTGCCTTGCGTC	X-*pilU* detect R
JCP314	GCAATTCGGAACTTGATCCGTG	*pilT*-X detect F
Point mutations		
Primer name	**Sequence (5' to 3')**	**Description**
BBC401	ACCAGCAAAGCTAATAAAATCGAG	*pilA* F
BBC404	CGCCATACTAACCCAATACACTC	*pilA* R
DOG0400	ACTTCTGGCTGAAGGTCAATTTTC	*pilTU* F
DOG0403	TCACGTGTTCGGCCAAAATC	*pilTU* R
ABD332	GGCTGAACGTGGTTGTCGAAAATGAC	*lacZ* F
ABD256	CCCAAATACGGCAACTTGGCG	*lacZ* R
HQP0002	CGCCAAGGTCGTCGAagcACCCGAGCCC	$pilT^{K136A}$ R1
HQP0001	GGGCTCGGGTgctTCGACGACCTTGGCG	$pilT^{K136A}$ F2
BBC2369	GGCTGCCATAGTGGTCGAggcACCCGAACCGGTTGCGC	$pilU^{K134A}$ R1
BBC2370	GCGCAACCGGTTCGGGTgccTCGACCACTATGGCAGCC	$pilU^{K134A}$ F2
BBC5056	CTTCTAATTTggCagCATATTCACTGCGCTGGGCATCATTCATGAT	$pilT^{E64A,E65A}$ R1
BBC5057	AGTGAATATGctGccAAATTAGAAGTCGATTTTTCTTTTGAACTGC	$pilT^{E64A,E65A}$ F2
BBC5059	GCACGCCAAGggcagcAACTTCGCCATCAATCCGTACCATAGGCGG	$pilT^{R35A,K36A}$ R1
BBC5060	TGGCGAAGTTgctgccCTTGGCGTGCCTGCTTTTACCCATTCTGAT	$pilT^{R35A,K36A}$ F2
ATP0076	AGTAACTCAGCGATggCCATTTAAATTCCTTAATAAAGTCTGGCTATGCGTAG	$pilT^{D2A}$ R1
ATP0075	AGGAATTTAAATGGccATCGCTGAGTTACTGGAATTTAGTGTAAAACATAACGC	$pilT^{D2A}$ F2
ATP0079	GCATCATTCATGATagCAAAAATCAAGCGATGTACATCAGAATGGGTAAAAGC	$pilT^{E53A}$ R1
ATP0078	TCGCTTGATTTTTGctATCATGAATGATGCCCAGCGCAGTGAATATGAA	$pilT^{E53A}$ F2
ATP0019	CGCCAAGCTTttcAACTTCGCCATCAATCCGTACCATAGGCGGAAC	$pilT^{R35E}$ R1
ATP0018	TGGCGAAGTTgaaAAGCTTGGCGTGCCTGCTTTTACCCATTCTGAT	$pilT^{R35E}$ F2
BBC5181	ACCATCGCTAtTtCATtTtAATCTTCACATTCTGCAAAGAGCCGC	$pilU^{D366K,E368K}$ R1
BBC5182	AAGATTaAaATGaAaTAGCGATGGTTACTTTGTGCGCTTTGC	$pilU^{D366K,E368K}$ F2
ATP0022	GCACGCCAAGtTcCCTAACTTCGCCATCAATCCGTACCATAGGCGG	$pilT^{K36E}$ R1
ATP0021	CGAAGTTAGGgAaCTTGGCGTGCCTGCTTTTACCCATTCTGATGTA	$pilT^{K36E}$ F2

ATP0025	ATCGCTACTCCATtTtAATCTTCACATTCTGCAAAGAGCCGCTGCCGTA	*pilU*^{D366K} R1
ATP0024	GAATGTGAAGATTaAaATGGAGTAGCGATGGTTACTTTGTGCGCTTTGC	*pilU*^{D366K} F2
ATP0028	AGTAACCATCGCTAtTtCATATCAATCTTCACATTCTGCAAAGAGC	*pilU*^{E368K} R1
ATP0027	TGAAGATTGATATGaAaTAGCGATGGTTACTTTGTGCGCTTTGCTT	*pilU*^{E368K} F2
ATP0046	AGTAACTCAGCGATtTtCATTTAAATTCCTTAATAAAGTCTGGCTATGCGTAG	*pilT*^{D2K} R1
ATP0045	AGGAATTTAAATGaAaATCGCTGAGTTACTGGAATTTAGTGTAAAACATAACGC	*pilT*^{D2K} F2
ATP0064	GCATCATTCATGATgcgAAAAATCAAGCGATGTACATCAGAATGGGTAAAAGC	*pilT*^{E53R} R1
ATP0063	TCGCTTGATTTTTcgcATCATGAATGATGCCCAGCGCAGTGAATATGAA	*pilT*^{E53R} F2
ATP0073	CACGCTTGGTaTcGAGCATCAAACGCAGATCGTTGGCTGAATCGGC	*pilU*^{K348D} R1
ATP0072	TTTGATGCTCgAtACCAAGCGTGGTGATGACTACGGCAGCGGCTCT	*pilU*^{K348D} F2
DOG0175	AAACTATCCAGATAAGGGAAAGC	*comP* (A. baylyi) F
DOG0178	AGGATCTGTAATGACGGGTTGAG	*comP* (A. baylyi) R
CE87	GAAGTTGTCGTACATTTCCAACATACAGCGCCACTAGCATATG	*comP*^{T129C} (A. baylyi) R1
CE88	CATATGCTAGTGGCGCTGTATGTTGGAAATGTACGACAACTTC	*comP*^{T129C} (A.baylyi) F2
BBC1934	GTTACAAAGTCAGGGACGTAAAG	*pilT/U* F (A. baylyi)
BBC1939	GGTATTCAGATTGATCGTCAGTTAG	*pilT/U* R (A. baylyi)
BBC2403	GCTGCAAGGGTGGTTGAagcACCGGAACCAGTGG	*pilT*^{K136A} R1 (A. baylyi)
BBC2404	CCACTGGTTCCGGTgctTCAACCACCCTTGCAGC	*pilT*^{K136A} F2 (A. baylyi)
ATP0096	CGAGTAATTCTGTTATtTtCATATTTTCCCCGAAGATCGTCAAAAGGTTTAATTATTTTG	*pilT*^{D2K} R1 (A. baylyi)
ATP0092	CGGGGAAAATATGcgTATAACAGAATTACTCGCGTTTTCGGTGC	*pilT*^{D2K} F2 (A. baylyi)
ATP0099	GTTTATCATTCATAATAcgGTAAATGAGATTATGGACTTCTGAATGATCCATTGCAG	*pilT*^{D53R} R1 (A. baylyi)
ATP0100	GTCCATAATCTCATTTACcgTATTATGAATGATAAACAGCGCCGAGACTACGAAG	*pilT*^{D53R} F2 (A. baylyi)
ATP0109	TCTTCCGAAAGaTcGATCTGTAGACGTAAATTATTAGGCGAGTCTGC	*pilU*^{K351D} R1 (A. baylyi)
ATP0110	GTCTACAGATCgAtCTTTCGGAAGAAGCCAACAAACCCCTAG	*pilU*^{K351D} F2 (A. baylyi)
HQP0004	GCGCAGTGAATATGAAGAG	*pilT*^{K136A} detect F
HQP0003	GCCAAGGTCGTCGGagc	*pilT*^{K136A} detect R
BBC2372	ATTTTGTATCGAGTCGATGGTG	*pilU*^{K134A} detect F
BBC2371	GCCATAGTGGTCGgggc	*pilU*^{K134A} detect R
BBC2386	tcactgcccgctttccagtcCTCAAGAATTGCCTCGACG	*pilT*^{E64A,E65A} detect F
BBC5058	AATCGACTTCTAATTTggtag	*pilT*^{E64A,E65A} detect R
BBC5061	TGATGGCGAAGTcgctgcc	*pilT*^{R35A,K36A} detect F

HQP0002	CGCCAAGGTCGTCGAagcACCCGAGCCC	*pilT*^{R35A,K36A} detect R
ATP0077	CAGACTTTATTAAGGAATTTAAATGacc	*pilT*^{D2A} detect F
ATP0080	GATGTACATCGCTTGATTTTTact	*pilT*^{E53A} detect F
ATP0020	ATTGATGGCGAAGTcgaa	*pilT*^{R35E} detect F
BBC5183	GCAGAATGTGAAGATTaAaATGaga	*pilU*^{D366K,E368K} detect F
ATP0023	GATGGCGAAGTTAGGgga	*pilT*^{K36E} detect F
ATP0026	TGCAGAATGTGAAGATTaga	*pilU*^{D366K} detect F
ATP0029	AGAATGTGAAGATTGATATGaga	*pilU*^{E368K} detect F
ATP0047	CAGACTTTATTAAGGAATTTAAATGaga	*pilT*^{D2K} detect F
ATP0065	GATGTACATCGCTTGATTTTccgc	*pilT*^{E53R} detect F
ATP0074	CTGCGTTTGATGCTCggt	*pilU*^{K348D} detect F
HQP0158	gtcgacggatccccggaatctaAATTTTGCTGAAGATTTCAGGAGC	*pilT* mutation detect R
DOG0407	TCATCAAGATAAGCATGAGTCAG	*pilU* mutation detect R
BBC2406	CAATGGATCATTCAGAAGTCC	*pilT*^{K136A} (A. baylyi) detect F
BBC2405	TGCAAGGGTGGTTGgagc	*pilT*^{K136A} (A. baylyi) detect R
CE89	TGCTAGTGGCGCTGTATGT	*comP*^{T129C} (A.baylyi) detect F
CE59	GCAATTAGCTCTTTATATAAAGTAG	*comP*^{T129C} (A.baylyi) detect R
ATP0095	GCTGCCCAAGTTGATACATC	*pilT*^{D2K} (A. baylyi) detect F
ATP0098	AACGCGAGTAATTCTGTTATtct	*pilT*^{D2K} (A. baylyi) detect R
DOG1040	ATTGACAGGGTTCTCATTTCAA	*pilT*^{D53R} (A. baylyi) detect F
ATP0101	CGCTGTTTATCATTCATAATgcg	*pilT*^{D53R} (A. baylyi) detect R
ATP0107	TACATGCCAATAATGCCAATC	*pilU*^{K351D} (A. baylyi) detect F
ATP0108	GGCTTCTTCCGAAAGtcc	*pilU*^{K351D} (A. baylyi) detect R

Movie S1. Representative movie of the montage shown in Fig S2a. mCherry-PilT^{+} does not form peripheral foci.

Movie S2. Representative movie of the montage shown in Fig S2a. mCherry-PilU^{+} does not form peripheral foci.

Movie S3. Representative movie of the montage shown in Fig 1b. Motor localization of mCherry-PilT^{WA} shows fluorescent foci at the cell poles.

Movie S4. Representative movie of the montage shown in Fig 1b. Motor localization of mCherry-PilU^{WA} foci shows fluorescent foci at the cell poles.

Movie S5. Representative movie of the montage from Fig S3a shows mCherry-PilT^{WA} and AF488-mal labeled pilus colocalization.

Movie S6. Representative movie of the montage from Fig S3a shows mCherry-PilU^{WA} and AF488-mal labeled pilus colocalization.

Movie S7. Representative movie of the montage from Fig S3b shows mCherry-PilT^{WA} and msfGFP-PilQ colocalization.

Movie S8. Representative movie of the montage from Fig S3b shows mCherry-PilU^{WA} and msfGFP-PilQ colocalization.

Movie S9. Representative movie of the montage from Fig 1e showing GFP-PilU^{WA} and PilT^{WA}-mCherry colocalization.

Movie S10. Molecular dynamics simulation of the AF3 PilT-PilU model. A 100-ns span of the simulation is shown for PilT^{R35}-PilU^{D366,E368}.

Movie S11. Molecular dynamics simulation of the AF3 PilT-PilU model. A 100-ns span of the simulation is shown for PilT^{R35}-PilU^{I365,M367}.

Movie S12. Molecular dynamics simulation of the AF3 PilT-PilU model. A 100-ns span of the simulation is shown for PilT^{K36}-PilU^{D366,E368}.

Movie S13. Molecular dynamics simulation of the AF3 PilT-PilU model. A 100-ns span of the simulation is shown for PilT^{D2,E53}-PilU^{K348}.

Dataset S1. Summary statistics and a comprehensive list of statistical comparisons for all quantitative data in the manuscript.